J. Appl. Comput. Mech., 11(2) (2025) 467-484
DOI: 10.22055/jacm.2024.47204.4674

ISSN: 2383-4536
jacm.scu.ac.ir

Shahid Chamran University of Ahvaz

Journal of Applied and Computational Mechanics

Research Paper

# Numerical Investigation on $Fe_3O_4$-Water Nanofluid in the Presence of Magnetotactic Bacteria

**Merve Gurbuz-Caldag, Bengisen Pekmen**

Department of Mathematics, TED University, Ankara, 06420, Turkey, Email: merve.gurbuz@tedu.edu.tr (M.G.C.); bengisenpekmen@gmail.com (B.P.)

Received June 17 2024; Revised August 06 2024; Accepted for publication August 27 2024.
Corresponding author: B. Pekmen (bengisenpekmen@gmail.com)


**Abstract.** In this study, numerical research on natural convection nanofluid flow in the presence of magnetotactic bacteria and $Fe_3O_4$-water is performed. The time independent, dimensionless governing equations involving nanoparticle concentration and the number of microorganisms is numerically solved by global radial basis function method with two distinct boundary conditions in a square cavity including double diffusivity or not. Streamlines, isotherms, isolines of concentration and bacteria are illustrated for a range of parameters including Rayleigh number ($10^2 \le Ra \le 10^5$), bioconvection Rayleigh number ($10 \le R_b \le 100$), Peclet number ($0.01 \le Pe \le 5$), Lewis number ($1 \le Le \le 10$) and buoyancy ratio number ($0.1 \le Nr \le 10$). To inspect how various parameters affect heat and mass transport, the average Nusselt ($\overline{Nu}$) and the average Sherwood ($\overline{Sh}$) numbers on the heated wall are tallied. It is found that in the case of first boundary condition, heat transfer diminishes 11.4%, 24.9%, 39.7%, as $Nr$, $R_b$, $Pe$ increases, and mass transfer rises 8.8%, 29.6% as $Nr$, $R_b$ increases. On the other hand, $\overline{Nu}$ increases 6.13% and $\overline{Sh}$ decreases 26.8% as $Le$ increments. In the case of second boundary condition, $\overline{Nu}$ and $\overline{Sh}$ rises with the augmentation of all physical parameters.

**Keywords:** $Fe_3O_4$-water, Magnetotactic bacteria, Nanofluid, Bioconvection, Natural convection.

## 1. Introduction

Nanofluids are obtained by adding small particles of nanometer size to base liquids such as oil, water, biofluids, and ethylene glycol. Many researchers have been interested in the heat and mass transfer of nanofluids due to technological applications in various fields such as biomechanics, science, nuclear industry, and chemistry. Additionally, nanofluid problems are utilized in engineering applications such as solar energy collection, heat exchangers, and cooling of electronic devices, etc. [1]. Choi and Eastman [2] firstly introduced the subject of nanofluids to improve the thermal conductivity. Heat transfer of nanofluid in a rectangular enclosure is analyzed by Khanafer et al. [3]. Finite volume approach is employed to get numerical results in terms of streamlines and isolines for different values of Grashof and Rayleigh numbers, and volume fractions. It is shown that nanoparticle volume fraction increases the rate of heat transfer. In [4], the simulations of copper-water nanofluid in different Rayleigh numbers are depicted with the application of the finite difference method. Kefayati [5] investigated the presence of oriented magnetic field on natural convection flow in a rectangular cavity filled by Cu-water nanofluid. Pekmen Geridonmez [6] utilized a radial basis function pseudo spectral method and differential quadrature method for the space and the time derivatives, respectively, to examine the natural convection nanofluid flow in case of distinct nanoparticles and aspect ratios. Bhuiyana et al. [7] studied the impacts of different water-based nanofluids on the heat transfer in a square cavity taking nanoparticles as Cu, Ag, $TiO_2$ and $Al_2O_2$. It is obtained that the heat transfer rate is higher for the nanofluid containing nanoparticles with high heat capacity. Joshi and Pattamatta [8] conducted an experimental study on the heat transfer of natural convection in a cavity filled by MWCNT-water nanofluid. It is reported that the rate of the heat transfer of MWCNT-water nanofluid is higher than the $Al_2O_3$-water nanofluid. In [9], the diesel oil with only molybdenum disulfide $MoS_2$ nanoparticles is searched. Friction factor is not influenced by addition of $MoS_2$ nanoparticles comparing to pure oil. Alsabery et al. [10] performed a numerical investigation on $Al_2O_3$-water nanofluid in a square cavity including rotating cylinder. Galerkin weighted residual method is employed to solve governing equations for the variations of physical parameters. The effect of zinc oxide ZnO and $MoS_2$ nanoparticles are compared inside diesel oil by Mousavi et al. [11]. It is found that the addition of ZnO nanoparticles is more effective on improved thermal properties. Mousavi and Heris [12] reported that viscosity, viscosity index, the flash point of the samples and the friction factor increase in addition of ZnO. In [13], the effect of ZnO and $MoS_2$ in host fluid diesel oil is also studied. Their results reveal that the friction factor increases by inclusion of nanoparticles to the host fluid. The influence of MWCNTs and $TiO_2$ nanoparticles in turbine meter oil is investigated in [14]. It is shown that MWCNTs highly reduces pressure comparing to $TiO_2$ inside turbine meter oil. In numerical part of the study, ANSYS is used. MWCNTs doped with $TiO_2$ and zinc Ferrite ($ZnFe_2O_4$) nanoparticles are experimentally investigated to enhance dielectric qualities of transformer oil by Pourpasha et al. [15]. Khouri et al. [16] studied graphene-oxide (GO) in a heat exchanger device. Based

Published online: September 01 2024

on experimental observations, a correlation for Nusselt number is derived. A synthetic lubricant as a synthesis of $Cu/TiO_2/MnO_2$-doped GO nanocomposites is proposed in [17].

Magnetite ($Fe_3O_4$) is used in drug delivery, photo-thermal therapy, biosensors, bioimaging, extraction of heavy metals, and tumor ablation therapy due to its strong magnetism, low toxicity, biocompatibility, and biodegradability [18, 19]. Sundar et al. [20] investigated experimentally the effective thermal conductivity and viscosity of the water-base fluid including $Fe_3O_4$ nanoparticles. The influence of oval heat source on the heat transfer in a rectangular cavity filled with $Fe_3O_4$-water nanofluid is studied by Moraveji and Hejazian [21]. Streamlines and isolines are depicted for different ranges of volume fraction of nanoparticles, Rayleigh number and the size of the heat source. In [22], various shaped obstacles (square, circular, diamond) in a square enclosure including Graphene/ $Fe_3O_4$-water hybrid nanofluid are examined considering uniform magnetic field and radiation. Galerkin finite element method (FEM) is performed, and the average Nusselt number along the bottom heated wall is found the largest in case of circular obstacles. $Fe_3O_4$-water nanofluid flow in a square cavity in the presence of uniform magnetic field and radiation is numerically (Galerkin FEM) studied comparing sinusoidally heated left and bottom walls with uniform heated ones [23]. It is shown that the uniform heated walls enhance heat transfer more than the nonuniform heated walls. Acharya [24] examined the diamond shaped multiple thermally nonconducting obstacles inside a square cavity filled with $Fe_3O_4$-water nanofluid under the effects of uniform magnetic field and radiation. Galerkin FEM is applied and sinusoidally heated left and bottom walls are set in square cavity. It is reported that the case of cold obstacles causes more heat transport. Tekir et al. [25] analyzed the impact of magnetic field on $Fe_3O_4$-Cu-water hybrid nanofluid in a circular pipe. The experimental results are achieved for various Reynolds numbers and nanoparticle volume concentrations. Eshgarf et al. [26] examined the experimental results of the viscosity and thermal conductivity of $Fe_3O_4$-water nanofluid and proposed a model using an artificial neural network (ANN). In this model, inputs are solid volume fraction and temperature, outputs are the viscosity and thermal conductivity of the nanofluid. In [27], four different cases of T-shaped rectangular fins inserted into two centrally fitted circular cylinders are numerically investigated in the presence of MWCNT- $Fe_3O_4$-water hybrid nanofluid. Galerkin FEM is performed in numerical calculations, and the maximum average Nusselt number is found in case of cross cooling and cross heating boundary conditions on cylinder. Galerkin FEM is also applied to simulate the natural convection flow of MWCNT- $Fe_3O_4$-water hybrid nanofluid in three different setups of micro wavy channels under the effect of uniform magnetic field [28]. It is found that the rise in amplitude of wavy wall results in heat transfer enhancement at the lower wavy surface.

Bioconvection is the convective motion of a fluid resulting from the directional swimming of microorganisms in the presence of gravity, magnetic field, oxygen or light. In literature, bioconvection problems are analyzed in different channels including gravitactic, oxytactic or gyrotactic bacteria. Alloui et al. [29] studied gravitactic bioconvection in a rectangular cavity. Contour plots of stream function, temperature and concentration are simulated in various physical parameters by implementing the control volume method. Bifurcation diagram of stream function is also examined. Kuznetsov [30] applied Galerkin finite element method to simulate the bioconvection problem with gyrotactic microorganisms in a horizontal layer. It is obtained that the impact of gyrotactic microorganisms is destabilizing. Kuznetsov [31] also performed a linear stability analysis of bioconvection flow containing oxytactic microorganism. Sheremet and Pop [32] investigated the heat and mass transfer of nanofluid including oxytactic bacteria in a square porous cavity. Streamlines, isotherms, isoconcentrations of oxygen and bacteria are depicted for various values of Rayleigh, bioconvection Rayleigh, Peclet, Lewis numbers utilizing finite difference method. They reported that average Nusselt number increases as Rayleigh number increases or Lewis number decreases. In [33], the effects of Schmidt and Peclet number are examined for unsteady boundary layer slip flow containing nanofluids and gyrotactic microorganisms over a stretching cylinder. Saini and Sharma [34] concerned the thermo-bioconvection in a porous media with gravitactic microorganisms. They stated that Lewis number increases the bioconvection. Heat transfer of natural convection flow in a square porus cavity filled by nanofluid containing oxytactic bacteria is investigated by Habibishandiz et al. [35]. FEM is employed to the nondimensional governing equations with constant and periodic temperature boundary conditions. They showed that microorganisms enhance the heat transfer in the case of periodic temperature distribution.

Magnetotactic bacteria (MTB) synthesize $Fe_3O_4$ and greigiteis $Fe_3S_4$ [36]. For that reason, they are used in biotechnological, nanotecnological, and medical applications. In [37], biosensors capable of detecting micron-sized biological entities are developed with the use of MTB. Benoit et al. [38] visualized tumors in mice utilizing magnetic resonance imaging where the positive contrast is provided by MTB. Also, there are some studies on the applications of MTB in bioremediation such as removal of heavy metals from wastewater [39, 40]. Pekmen et al. [41] studied magnetotactic bacteria inside $Fe_3O_4$-water nanofluid in a wavy cavity under the effects of uniform magnetic field, Thermophoresis and Brownian effects are taken into account, and assumed that the bacteria are fed by nanoparticle $Fe_3O_4$. It is shown that the flux density of microorganism is reduced by the rise in Peclet number.

As seen in the literature, there are many studies on the heat and mass transfer of nanofluids including $Fe_3O_4$ nanoparticles or bioconvection problems including different microorganisms. However, the heat and mass transfer of nanofluid including MTB has not been studied yet. Within this motivation, $Fe_3O_4$-water nanofluid including MTB is considered in a square cavity with different boundary conditions. $Fe_3O_4$ is taken for a nanoparticle since MTB synthesize $Fe_3O_4$ and we assume that MTB live in $Fe_3O_4$ water consuming it, too. The current study focuses on the analysis of stream function, temperature, concentration and the number of bacteria for various physical parameters which are Rayleigh, bioconvection Rayleigh, Peclet, Lewis numbers and buoyancy ratio parameter. Also, the impacts of variables on the heat and mass transfer are examined for different boundary conditions.

## 2. The Considered Problem

The two-dimensional, time independent natural convection flow in a unit square cavity filled with $Fe_3O_4$-water is considered in the presence of magnetotactic bacteria. The problem is configured in Fig. 1. The two distinct boundary conditions are demonstrated in this figure by BC1 (left) and BC2 (right) configurations. The left wall is the heated wall while the right wall is the cold wall. The top and the bottom walls are insulated walls. It is assumed that $Fe_3O_4$ concentration is independently added to the system as a concentration existing in double-diffusive natural convection flow, and the magnetotactic bacteria consumes $Fe_3O_4$.

Buoyancy effect is included by Boussinesq approximation due to the temperature difference and density difference as well. The Joule heating effect, the viscous dissipation and the radiation effect are neglected. Thermophoresis and Brownian motion effects are also ignored.

A single-phase model for $Fe_3O_4$-water nanofluid is used and the physical properties can be formulated as [3]:

$$\rho_{nf} = (1-\phi)\rho_f + \phi\rho_s, \tag{1}$$

$$(\rho c_p)_{nf} = (1-\phi)(\rho c_p)_f + \phi(\rho c_p)_s, \tag{2}$$

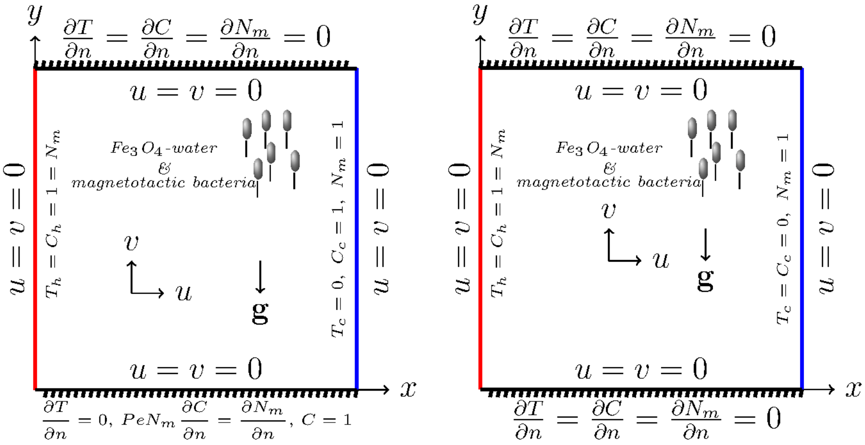


**Fig. 1.** Problem configuration with BC1 (left) and BC2 (right).

$$(\rho\beta)_{nf} = (1-\phi)(\rho\beta)_f + \phi(\rho\beta)_s, \tag{3}$$

$$\alpha_{nf} = \frac{k_{nf}}{(\rho c_p)_{nf}}, \tag{4}$$

where subindices *nf, f, s* denote the nanofluid, fluid and solid, respectively, $\rho$ is the density, $\beta$ is the thermal expansion coefficient, $c_p$ is the specific heat, $\alpha$ is the thermal diffusivity and $\phi$ is the solid volume fraction.

Nanofluid thermal conductivity $k_{nf}$ reported in [42] is taken as:

$$\frac{k_{nf}}{k_f} = \frac{k_s + 2k_f - 2\phi(k_f - k_s)}{k_s + 2k_f + \phi(k_f - k_s)}, \tag{5}$$

and the dynamic viscosity of nanofluid $\mu_{nf}$ modeled by Brinkman [43] is provided as:

$$\mu_{nf} = \mu_f(1-\phi)^{-2.5}. \tag{6}$$

Thermophysical properties of water and $Fe_3O_4$ tabulated by Pekmen and Oztop [41] are depicted in Table 1. The dimensional equations which are the combinations of the given references [30, 41, 44, 45, 46] are comprised of continuity, momentum, energy, nanoparticle concentration and the number of microorganisms as follows:

$$\frac{\partial u'}{\partial x'} + \frac{\partial v'}{\partial y'} = 0, \tag{7}$$

$$\nu_{nf}\nabla^2 u' = u'\frac{\partial u'}{\partial x'} + v'\frac{\partial u'}{\partial y'} + \frac{1}{\rho_{nf}}\frac{\partial p'}{\partial x'}, \tag{8}$$

$$\nu_{nf}\nabla^2 v' = u'\frac{\partial v'}{\partial x'} + v'\frac{\partial v'}{\partial y'} + \frac{1}{\rho_{nf}}\frac{\partial p'}{\partial y'} + \frac{g}{\rho_{nf}}\left(\gamma\Delta\rho n' - (\rho\beta)_{nf}(T' - T_c) + (\rho_s - \rho_f)\beta_s(C' - C^*)\right), \tag{9}$$

$$\alpha_{nf}\nabla^2 T' = u'\frac{\partial T'}{\partial x'} + v'\frac{\partial T'}{\partial y'}, \tag{10}$$

$$D_c\nabla^2 C' = u'\frac{\partial C'}{\partial x'} + v'\frac{\partial C'}{\partial y'} + \delta n', \tag{11}$$

$$\frac{\partial}{\partial x'}\left(u'n' + \frac{bW_c}{\Delta C'}\frac{\partial C'}{\partial x'}n' - D_n\frac{\partial n'}{\partial x'}\right) + \frac{\partial}{\partial y'}\left(v'n' + \frac{bW_c}{\Delta C'}\frac{\partial C'}{\partial y'}n' - D_n\frac{\partial n'}{\partial y'}\right) = 0, \tag{12}$$

**Table 1.** Thermophysical properties of water and $Fe_3O_4$ [41].

| Property | Water | $Fe_3O_4$ |
|---|---|---|
| $\rho$ (kg/m$^3$) | 997.1 | 5200 |
| $c_p$ (J/(kgK) | 4179 | 670 |
| k (W/(mK)) | 0.613 | 6 |
| $\beta\times10^{-5}$ (1/K) | 21 | 1.3 |

where $\nu$ is the kinematic viscosity, $u'$ and $v'$ are velocity components, $p'$ is the pressure, $g$ is the gravitational acceleration, $\gamma$ is the mean volume of microorganism, $D_c$ is the diffusivity of nanoparticle concentration, $n$ is the density/number of bacteria, $W_c$ is the maximum cell swimming speed, $b$ is the chemotaxis constant, $D_n$ is the diffusivity of microorganism, $T'$ is the temperature, $C'$ is the concentration, $\delta n'$ is the $Fe_3O_4$ consumption by the bacteria, $\Delta C' = C_h - C^*$ and $\Delta\rho' = \rho_{cell} - \rho_{nf}$. $C^* = C_{min}$ and $C_c$ for BC1 and BC2, respectively.

The non-dimensional transformation parameters are introduced as:

$$(x,y) = \frac{1}{L}(x',y'),\ (u,v) = \frac{L}{\alpha_f}(u',v'),\ p = \frac{L^2}{\rho_f \alpha_f^2}p',\ T = \frac{T' - T_c}{\Delta T},\ C = \frac{C' - C^*}{\Delta C},\ N_m = \frac{n'}{n_0},$$

where $L$ is the characteristic length, $\Delta T$ is the temperature difference between the hot and the cold walls, $\Delta C$ is the concentration difference and $n_0$ is the reference average number of bacteria.

By means of these parameters in dimensional equations, non-dimensional equations are achieved by:

$$\frac{\partial u}{\partial x} + \frac{\partial v}{\partial y} = 0 \tag{13}$$

$$\frac{\nu_{nf}}{\nu_f} Pr\nabla^2 u = u\frac{\partial u}{\partial x} + v\frac{\partial u}{\partial y} + \frac{\rho_f}{\rho_{nf}}\frac{\partial p}{\partial x}, \tag{14}$$

$$\frac{\nu_{nf}}{\nu_f} Pr\nabla^2 v = u\frac{\partial v}{\partial x} + v\frac{\partial v}{\partial y} + \frac{\rho_f}{\rho_{nf}}\frac{\partial p}{\partial y} - \frac{(\rho\beta)_{nf}}{\rho_{nf}\beta_f}RaPrT + \frac{\rho_f}{\rho_{nf}}RaPr(R_b N_m + NrC), \tag{15}$$

$$\frac{\alpha_{nf}}{\alpha_f}\nabla^2 T = u\frac{\partial T}{\partial x} + v\frac{\partial T}{\partial y}, \tag{16}$$

$$\frac{1}{Le}\nabla^2 C = u\frac{\partial C}{\partial x} + v\frac{\partial C}{\partial y} + \frac{\sigma}{Le}N_m, \tag{17}$$

$$\frac{1}{Le}\nabla^2 N_m = \chi\left(u\frac{\partial N_m}{\partial x} + v\frac{\partial N_m}{\partial y}\right) + \frac{Pe}{Le}\left(N_m\nabla^2 C + \frac{\partial C}{\partial x}\frac{\partial N_m}{\partial x} + \frac{\partial C}{\partial y}\frac{\partial N_m}{\partial y}\right), \tag{18}$$

where $\chi = D_c / D_n$, $\sigma = \delta n_0 L^2 / D_c \Delta C$ and $N_m$ is the number of microorganisms. Prandtl, Rayleigh, bioconvection Rayleigh, Peclet numbers, buoyancy ratio parameter and Lewis numbers have the following definitions:

$$Pr = \frac{\nu_f}{\alpha_f},\ Ra = \frac{g\beta_f \Delta T L^3}{\nu_f \alpha_f},\ R_b = \frac{\gamma\Delta\rho n_0}{\rho_f \beta_f \Delta T},\ Pe = \frac{bW_c}{D_n},\ Nr = \frac{(\rho_s - \rho_f)\beta_s \Delta C}{\rho_f \beta_f \Delta T},\ Le = \frac{\alpha_f}{D_c}.$$

The use of the formulations of stream function $(u,v) = (\partial\psi/\partial y, -\partial\psi/\partial x)$ and vorticity $\omega = \partial v/\partial x - \partial u/\partial y$ gives the governing non-dimensional equations as follows:

$$\nabla^2\psi = -\omega, \tag{19}$$

$$\frac{\alpha_{nf}}{\alpha_f}\nabla^2 T = u\frac{\partial T}{\partial x} + v\frac{\partial T}{\partial y}, \tag{20}$$

$$\frac{1}{Le}\nabla^2 C = u\frac{\partial C}{\partial x} + v\frac{\partial C}{\partial y} + \frac{\sigma}{Le}N_m, \tag{21}$$

$$\frac{1}{Le}\nabla^2 N_m = \chi\left(u\frac{\partial N_m}{\partial x} + v\frac{\partial N_m}{\partial y}\right) + \frac{Pe}{Le}\left(N_m\nabla^2 C + \frac{\partial C}{\partial x}\frac{\partial N_m}{\partial x} + \frac{\partial C}{\partial y}\frac{\partial N_m}{\partial y}\right), \tag{22}$$

$$\frac{\nu_{nf}}{\nu_f} Pr\nabla^2\omega = u\frac{\partial\omega}{\partial x} + v\frac{\partial\omega}{\partial y} - \frac{(\rho\beta)_{nf}}{\rho_{nf}\beta_f}RaPr\frac{\partial T}{\partial x} + \frac{\rho_f}{\rho_{nf}}RaPr\left(R_b\frac{\partial N_m}{\partial x} + Nr\frac{\partial C}{\partial x}\right). \tag{23}$$

Two cases of boundary conditions are settled. The first boundary conditions (BC1) are considered as in oxytactic bacteria [32] (as a difference $Nr$ is taken into account in the current study), and the second boundary conditions are considered as in double diffusive [45, 47, 48]. These two cases may be stated as follows:

BC1:

$$\text{on}\quad x = 0:\ u = v = \psi = 0,\ T = 1,\ C = N_m = 1, \tag{24}$$

$$\text{on}\quad x = 1:\ u = v = \psi = 0 = T,\ C = N_m = 1, \tag{25}$$

$$\text{on}\quad y=0: u=v=\psi=0,\ \frac{\partial T}{\partial y}=0,\ C=1,\ PeN_m\frac{\partial C}{\partial y}=\frac{\partial N_m}{\partial y}, \tag{26}$$

$$\text{on}\quad y=1\ : u=v=\psi=0,\ \frac{\partial T}{\partial y}=\frac{\partial C}{\partial y}=\frac{\partial N_m}{\partial y}=0. \tag{27}$$

BC2:

$$\text{on}\quad x=0: u=v=\psi=0,\ T=C=N_m=1, \tag{28}$$

$$\text{on}\quad x=1: u=v=\psi=0=T=C,\ N_m=1, \tag{29}$$

$$\text{on}\quad y=0: u=v=\psi=0,\ \frac{\partial T}{\partial y}=\frac{\partial C}{\partial y}=\frac{\partial N_m}{\partial y}=0, \tag{30}$$

$$\text{on}\quad y=1: u=v=\psi=0,\ \frac{\partial T}{\partial y}=\frac{\partial C}{\partial y}=\frac{\partial N_m}{\partial y}=0. \tag{31}$$

The average Nusselt and average Sherwood numbers along the heated left wall are computed from:

$$\overline{Nu}=-\frac{k_{nf}}{k_f}\int_0^1\frac{\partial T}{\partial x}dy,\quad \overline{Sh}=-\int_0^1\frac{\partial C}{\partial x}dy. \tag{32}$$

where $\overline{Nu}$ and $\overline{Sh}$ are the ratio of convective heat transfer to conductive heat transfer, and convective mass transfer to conductive mass transfer, respectively.

## 3. Numerical Method

Radial basis function (RBF) method [49, 50] is based on the collocation technique where the domain and the boundary of the region of the problem are discretized by $N_d$ and $N_b$ points. In this method, the unknown $\xi$ is approximated by RBF $g(r)$:

$$\xi(x,y)=\sum_{i=1}^{N_d+N_b}a_i g(\|x-x_i\|), \tag{33}$$

in which $r=\|x-x_i\|$ represents the Euclidean norm of the field $x$ and collocation points $x_i$. The collocation form of Eq. (33) is stated as:

$$\xi=Ga, \tag{34}$$

where the dimensions of matrix $G$ and the vector $a$ are $(N_d+N_b)\times(N_d+N_b)$ and $(N_d+N_b)\times 1$, respectively.

The partial derivatives of $\xi$ acquired from the equations Eq. (33) and Eq. (34) can be expressed as follows:

$$\frac{\partial \xi}{\partial x}=\frac{\partial G}{\partial x}G^{-1}\xi,\quad \frac{\partial \xi}{\partial y}=\frac{\partial G}{\partial y}G^{-1}\xi, \tag{35}$$

$$\frac{\partial^2 \xi}{\partial x^2}=\frac{\partial^2 G}{\partial x^2}G^{-1}\xi,\quad \frac{\partial^2 \xi}{\partial y^2}=\frac{\partial^2 G}{\partial y^2}G^{-1}\xi, \tag{36}$$

wherein the matrices $G_x, G_y, G_{xx}$ and $G_{yy}$ are constructed by taking the corresponding partial derivatives of RBF $g(r)$. In the current study, polyharmonic spline RBF $g(r)=r^7$ is employed to solve the equations Eqs. (19) to (23) and the discretized form can be written as:

$$P_L\psi^{k+1}=-\omega^k, \tag{37}$$

$$\left(\frac{\alpha_{nf}}{\alpha_f}P_L-K\right)T^{k+1}=0, \tag{38}$$

$$(P_L-LeK)C^{k+1}=\sigma N_m^k, \tag{39}$$

$$\left(P_L-Le\chi K-PeP_L[C^{k+1}]_d-Pe(P_x[C^{k+1}]_dP_x+[P_yC^{k+1}]_dP_y)\right)N_m^{k+1}=0, \tag{40}$$

$$\left(\frac{\nu_{nf}}{\nu_f}PrP_L-K\right)\omega^{k+1}=-\frac{(\rho\beta)_{nf}}{\rho_{nf}\beta_f}RaPrP_xT^{k+1}+\frac{\rho_f}{\rho_{nf}}RaPr(R_bP_xN_m^{k+1}+NrP_xC^{k+1}), \tag{41}$$

where $K=([P_y\psi]_dP_x+[P_x\psi]_dP_y)$, $P_x=G_xG^{-1}$, $P_y=G_yG^{-1}$ and $P_L=(G_{xx}+G_{yy})G^{-1}$. $[.]_d$ represents the diagonal matrix, $k$ denotes the iteration level. Iteration continues until the stopping condition:

$$\sum_{Y=\psi,T,C,N_m,\omega} \frac{\| Y^{k+1} - Y^k \|_\infty}{\| Y^{k+1} \|_\infty} < \varepsilon = 10^{-5}, \tag{42}$$

is hold. In this iteration process, vorticity boundary conditions are acquired from the vorticity definition as:

$$\omega^{k+1} = P_x v^{k+1} - P_y u^{k+1}, \tag{43}$$

and relaxation parameter $\tilde{\gamma}$ is used for the vorticity such that:

$$\omega^{k+1} = (1-\tilde{\gamma})\omega^k + \tilde{\gamma}\omega^{k+1}. \tag{44}$$

In the Eq. (32), $\overline{Nu}$ and $\overline{Sh}$ are evaluated utilizing the Composite Simpson's 1/3 rule for the integration.

## 4. Some Numerical Observations

RBF method is implemented in-house codes in MATLAB to obtain numerical results in an Intel Core i5 computer with 8 GB RAM. In all numerical calculations, a uniform mesh generation is done, and all figures are sketched in MATLAB by using interpolation and contour plots.

### 4.1. Validation

The present numerical process is validated by two problems. In the first one, conventional natural convection flow in a square cavity is solved, and the computed average Nusselt numbers along the heated left wall are compared with Davis [51] in Table 2. Our results are in good agreement with results in [51]. In the second comparison, a bioconvection problem solved in [32] is solved, and the found $\overline{Nu}$ and $\overline{Sh}$ values along the heated left vertical wall are compared. Table 3 depicts that our results are in good harmony with these results.

The global RBF is also validated with an experimental work presented in Ho et al. [52]. In order to be able to compare the current process in large $Ra_{nf}$ numbers as multiples of $10^7$, the uniform nodes are made denser close to the walls. Table 4 shows the success of the present numerical method for getting close results to an experimental study. In this Table, $N$ corresponds to the number of points in one side wall. FEM application in Saghir et al. [53] to the same experimental problem is also inserted to see good catch in our results.

### 4.2. Grid Independency

Grid independence is checked in Table 5 in both BC cases. Regarding to this table results, $41\times41$ number of uniform grid points are used at all computations.

**Table 2.** Validation with Davis using 41×41 uniform nodes.

| | Davis [51] | Current Study |
|---|---|---|
| $Ra$ | $\overline{Nu}$ | $\overline{Nu}$ |
| $10^3$ | 1.117 | 1.118 |
| $10^4$ | 2.238 | 2.243 |
| $10^5$ | 4.509 | 4.474 |

**Table 3.** Validation with Sheremet and Pop [32]

| | | | | Sheremet and Pop [32] | | Current Study | |
|---|---|---|---|---|---|---|---|
| $Ra$ | $Rb$ | $Le$ | $Pe$ | $\overline{Nu}$ | $\overline{Sh}$ | $\overline{Nu}$ | $\overline{Sh}$ |
| 10 | 10 | 1 | 0.1 | 1.0775 | 0.3368 | 1.0772 | 0.3366 |
| | | | 1 | 1.0720 | 0.3296 | 1.0715 | 0.3293 |
| | | 10 | 0.1 | 1.0771 | 0.2556 | 1.0769 | 0.2553 |
| | | | 1 | 1.0397 | 0.2298 | 1.0393 | 0.2295 |
| | 100 | 1 | 0.1 | 1.0717 | 0.3447 | 1.0711 | 0.3444 |
| | | | 1 | 1.1723 | 0.3650 | 1.1806 | 0.3675 |
| 100 | 10 | 1 | 0.1 | 3.0910 | 0.2506 | 3.1236 | 0.2494 |
| | | | 1 | 2.6560 | 0.2270 | 2.6563 | 0.2261 |

**Table 4.** An experimental study comparison on average Nusselt number.

| $Ra_{nf}$ | $Pr_{nf}$ | $\phi$ | Ho et al. [52] | Saghir et al. [53] | Present ($N$ = 37) | Present ($N$ = 41) |
|---|---|---|---|---|---|---|
| 7.7455e+7 | 7.0659 | 0.01 | 32.2037 | 31.8633 | 32.9760 | 31.8101 |
| 6.6751e+7 | 7.3593 | 0.02 | 31.0905 | 31.6085 | 30.7871 | 29.9145 |
| 5.6021e+7 | 7.8353 | 0.03 | 29.0769 | 28.2160 | 28.4236 | 27.8218 |

**Table 5.** Grid Independency when $R_b$ = 10, $Le$ = $Pe$ = $Nr$ = 1.

| | | BC1 | | BC2 | |
|---|---|---|---|---|---|
| $Ra$ | $N \times N$ | $\overline{Nu}$ | $\overline{Sh}$ | $\overline{Nu}$ | $\overline{Sh}$ |
| | 31×31 | 1.73339 | 0.279724 | 1.78063 | 2.10257 |
| $10^4$ | 41×41 | 1.72828 | 0.279921 | 1.79492 | 2.11559 |
| | 51×51 | 1.72653 | 0.279993 | 1.79961 | 2.11994 |

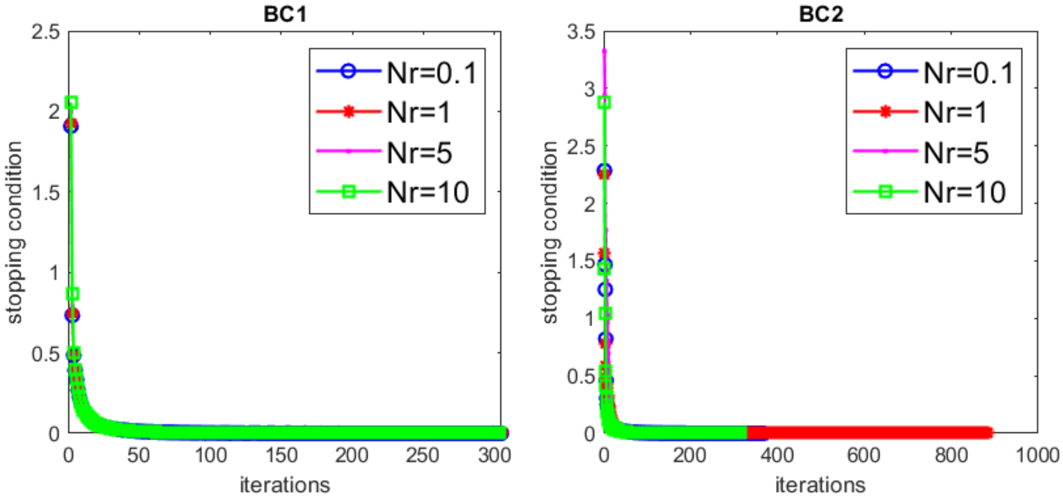


**Fig. 2.** Stopping condition (Eq. (42)) vs iterations in different $Nr$ values for $Ra = 10^4$, $R_b = 10$, $Pe = Le = 1$.

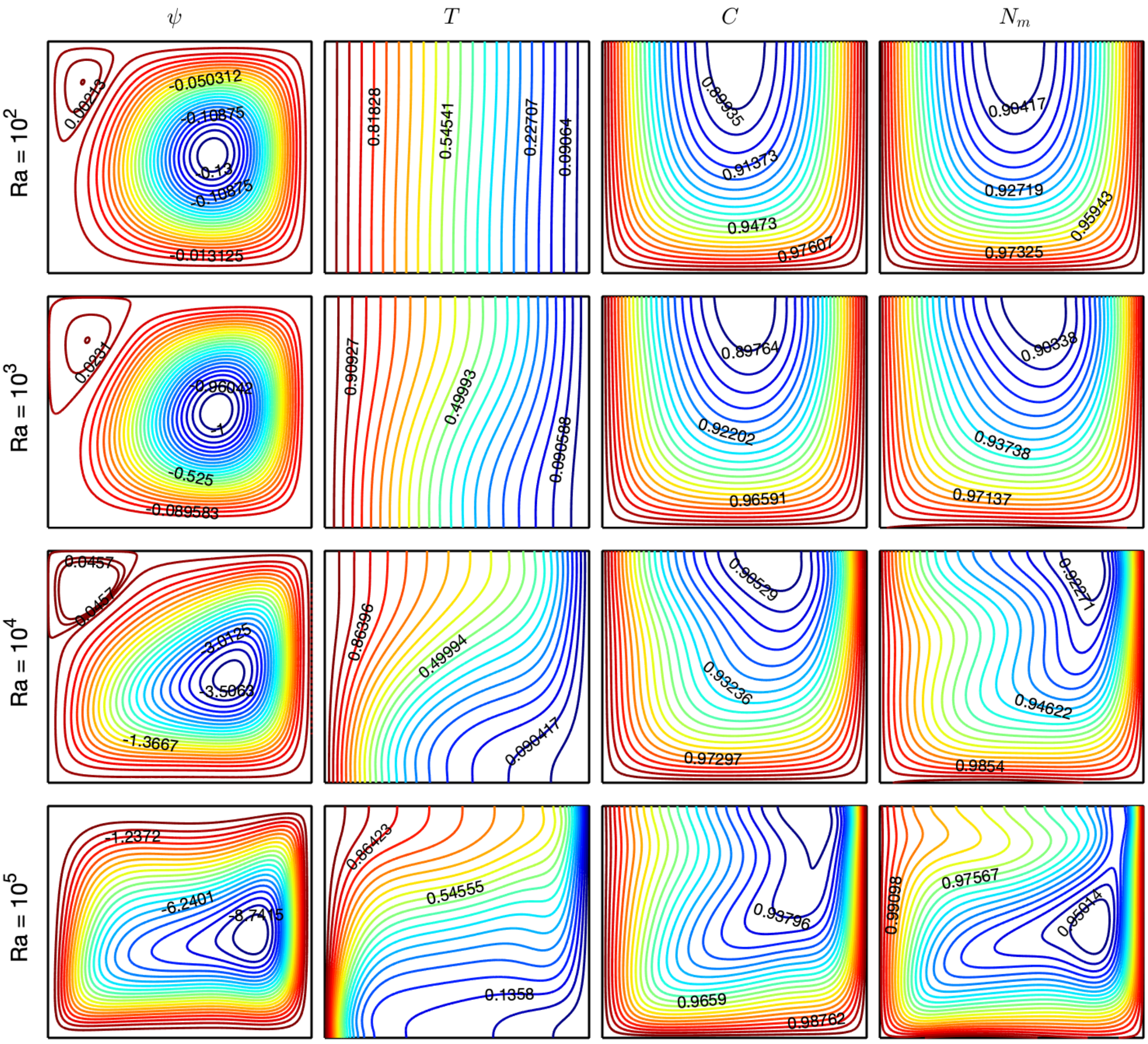


**Fig. 3.** The effect of $Ra$ for $R_b = 10$, $Pe = Le = Nr = 1$ in BC1 case.

In the following parts, some numerical results are displayed both in isolines and tabular representations. Prandtl number is fixed at 6.8. $\chi = 1$ is taken, namely, $D_n = D_c$ diffusivity of bacteria is the same as the diffusivity of nanoparticle concentration. $\sigma$ is set to be 1. Based on literature investigations, the range of the parameters is chosen as $10^2 \le Ra \le 10^5$, $10 \le R_b \le 100$, $0.1 \le Nr \le 10$, $0.1 \le Pe \le 5$, $1 \le Le \le 10$. Figures 3-7 are obtained by considering BC1, and the remaining figures are for BC2. In these results, the concentration of nanoparticle concentration is held at $\phi = 0.02$. In these figures, streamlines $(\psi)$, isotherms $(T)$, isoconcentration lines $(C)$, and isolines for density of bacteria $(N_m)$ are illustrated column wise. Figure 2 presents the stopping condition (Eq. (42)) vs iterations in different $Nr$ values in both BC cases.

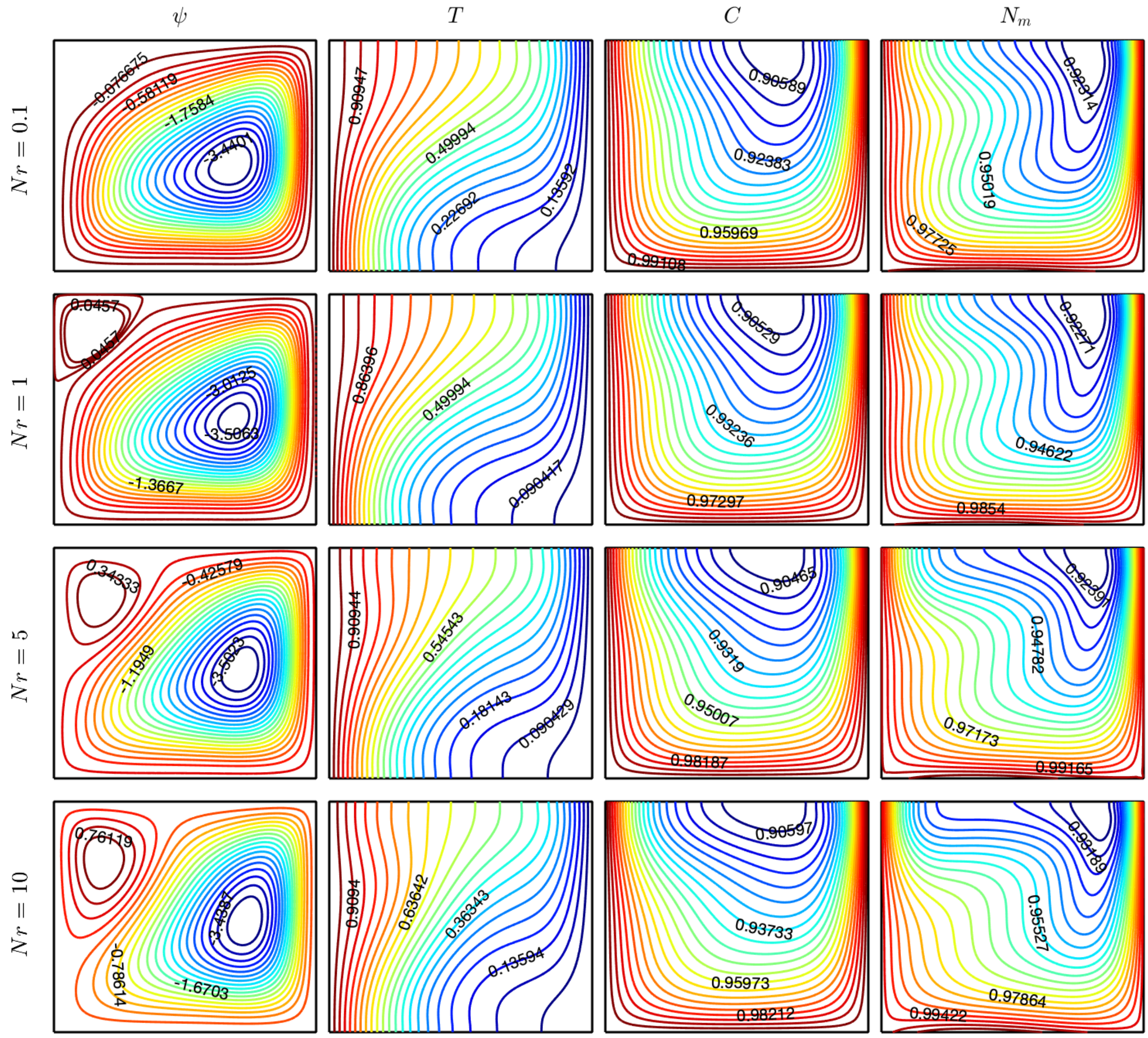


**Fig. 4.** The effect of *Nr* for $Ra = 10^4$, $R_b = 10$, $Pe = Le = 1$ in BC1 case.

### 4.3. BC1 results

In this section, numerical results with BC1 are examined. Figure 3 analyzes the Rayleigh number variation keeping $R_b = 10$, $Pe = Le = Nr = 1$. The rise in $Ra$ number results in more natural convective behavior. In streamlines, counter rotating primary cell at $Ra = 10^5$ annihilates the secondary cell seen at smaller $Ra$ numbers. This is a result of the dominancy of buoyancy force on the presence of bioconvective behavior ($Ra = 10^5$ dominates over $R_b = 10$). In isotherms, thermal boundary layers obviously appear along the vertical walls confirming the rise in convection at $Ra = 10^5$. Nanoparticle concentration isolines develop solutal boundary layers at $Ra = 10^3, 10^4$ along the vertical walls while the left solutal boundary layer lessens as $Ra$ increases more. Magnetotactic bacteria accumulated through the top wall at $Ra = 10^2$ moves down at $Ra = 10^3, 10^4$, and form a cell close to the right wall at $Ra = 10^5$ which may be due to the strong press of primary cell through the right wall.

In Table 6, $\psi_{\min}$ also verifies rapid fluid flow as $Ra$ rises. The convective heat transfer gets higher due to the rise in buoyancy force but convective mass transfer decreases. Maximum number of magnetotactic bacteria firstly rises from $10^2$ to $10^3$, but then it is decreasing from $10^3$ to $10^5$.

In Fig. 4. the impact of buoyancy ratio term is scrutinized holding $Ra = 10^4$, $R_b = 10$, $Pe = Le = 1$. By definition of $Nr$, the larger the $Nr$ is, the larger the concentration effect is expected. In streamlines primary cell is shrunk, and secondary cell grows up. In isotherms, thermal boundary layers in small bold isolines along the left and the right walls at $Nr = 0.1$ are declined with the rise in $Nr$. In isoconcentration lines, small solutal layer at the left top corner becomes more prominent at $Nr = 10$ pointing to the rise in mass transfer. A similar behavior occurs in $N_m$ isolines. Table 7 confirms the rise in fluid flow both in primary and secondary cells by the increasing values of $\psi_{\min}$ and $\psi_{\max}$. $\overline{Nu}$ is reduced 11.4 % and $\overline{Sh}$ rises 8.8 % from $Nr = 0.1$ to $Nr = 10$. The number of bacteria also gets up a little bit with the rise in buoyancy force resulted with nanoparticle concentration. This may be due to the rise in consumption of nanoparticles by MTB.

**Table 6.** The effect of *Ra* for $R_b = 10$, $Pe = Le = Nr = 1$ in BC1 case.

| $Ra$ | $\psi_{\min}$ | $\psi_{\max}$ | $N_m^{\max}$ | $\overline{Nu}$ | $\overline{Sh}$ | CPU (sec) |
|---|---|---|---|---|---|---|
| $10^2$ | -0.13448 | 0.00376 | 1.00089 | 1.04669 | 0.34308 | 326.016 |
| $10^3$ | -1.03811 | 0.04570 | 1.00537 | 1.11561 | 0.32999 | 311.219 |
| $10^4$ | -3.60155 | 0.16015 | 1.00498 | 1.72828 | 0.27992 | 295.766 |
| $10^5$ | -9.15659 | 0.01288 | 1.00374 | 3.87422 | 0.22328 | 871.141 |

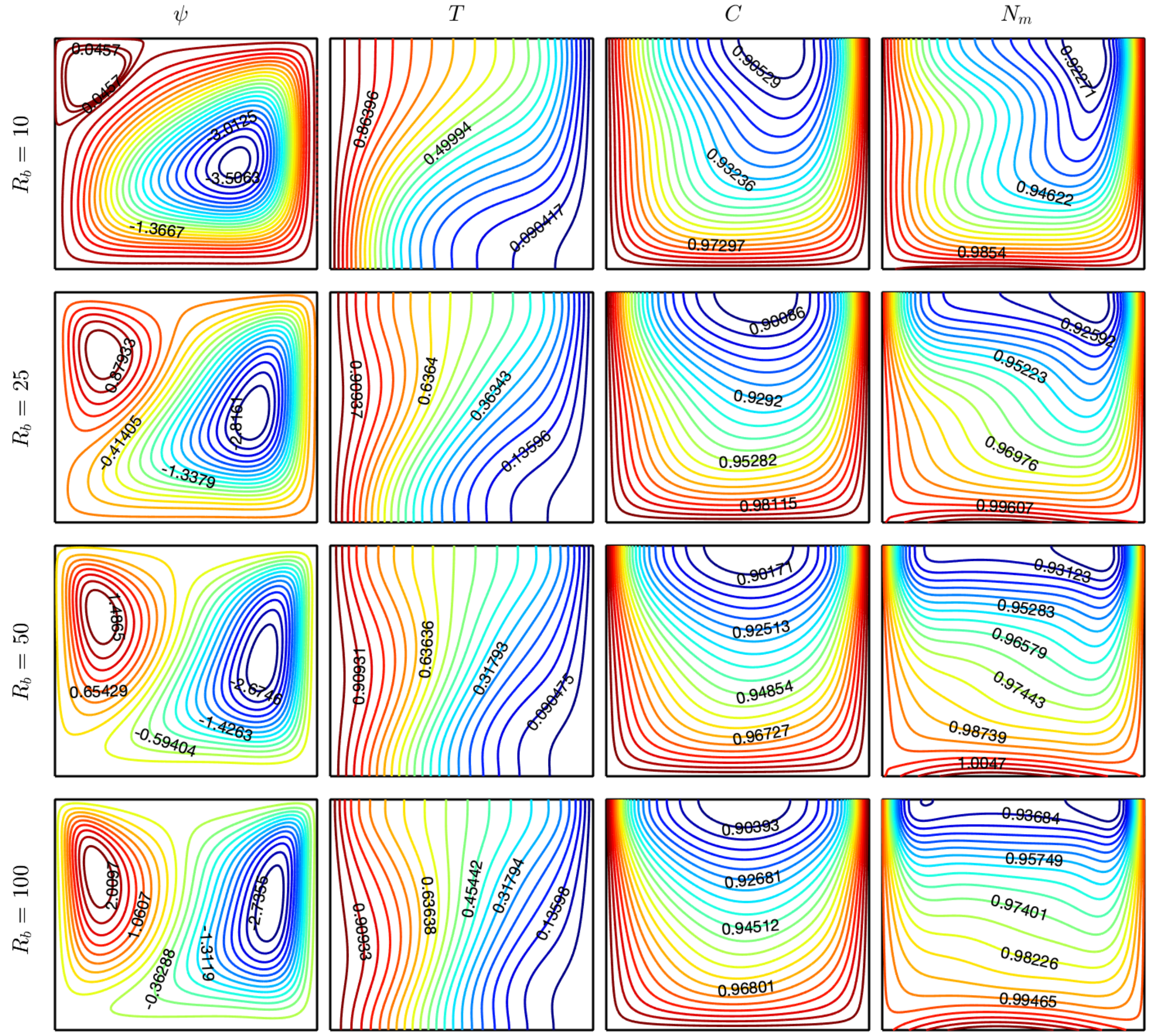


**Fig. 5.** The effect of $R_b$ for $Ra$ = $10^4$, $Pe$ = $Le$ = $Nr$ = 1 in BC1 case.

Bioconvection Rayleigh number alteration is observed in Fig. 5. with $Ra = 10^4, Pe = Le = Nr = 1$. The definition of $R_b$ indicates that the larger the $R_b$ is, the larger the average volume of bacteria arises. The augmentation of $R_b$ squeezes the primary cell with a decreasing magnitude, but enlarges the secondary cell which produces a counter rotating force as indicated in the momentum equation. Convective behavior in isotherms at $R_b = 10$ from the left hot wall to the right cold wall is distorted as $R_b$ grows. In isoconcentration lines, solutal boundary layer at the top left corner at $R_b = 10$ becomes more remarkable at $R_b = 100$, and symmetrically formed solutal layers along the vertical walls prevail. Magnetotactic bacteria moving down at $R_b = 10$ spread along the top wall as $R_b$ increases. In Table 8, the decrease and the increase in fluid velocities in primary and in secondary cells, respectively, are obviously seen in $\psi_{min}$ and $\psi_{max}$ values as $R_b$ increases up to 100. The number of bacteria is increasing as $R_b$ increases. From $R_b = 10$ to $R_b = 100$, $\overline{Nu}$ decreases 24.9 % while $\overline{Sh}$ increases 29.98 %.

The change in Peclet number is observed in Fig. 6. when $Ra = 10^4, R_b = 10, Le = Nr = 1$. The larger the $Pe$ is, the larger the maximum cell swimming speed or the slower the bacteria diffuse. Note that diffusivity of bacteria term $D_n$ in $Pe$ number and the diffusivity of nanoparticle concentration $D_c$ are assumed the same. That is, if $Le$ number is fixed in $Pe$ variation, it means that $Pe$ only varies directly with maximum cell swimming speed. In streamlines, the secondary cell increases at $Pe = 1$ and $Pe = 5$ while the primary cell is suppressed to the right wall of the cavity. In isotherms, the thermal boundary layers along the vertical walls decreases as $Pe$ rises. That is, the natural convection decreases. Solutal boundary layer along the left and the bottom wall at $Pe = 0.1$ decreases a little bit at $Pe = 1$, but it becomes thicker along the vertical walls at $Pe = 5$ indicating the enhancement in mass transfer. Downward acting bacteria at $Pe = 0.1$ moves upward fast and spread along the top wall at $Pe = 5$ which may be due to the rise in maximum cell swimming speed at $Pe = 5$. In Table 9 the decrease in fluid velocity in primary cell and the increase in secondary cell are verified by $\psi_{min}$ and $\psi_{max}$ values. The number of bacteria is rising a little bit from $Pe = 0.1$ to $Pe = 3$, but then it decreases 32.5 % from $Pe = 3$, to $Pe = 5$. Convective heat transfer decreases 39.7 % from $Pe = 0.1$ to $Pe = 5$. Convective mass transfer decreases from $Pe = 0.1$ to $Pe = 1$ firstly, but then it increases 7.36 % from $Pe = 1$ to $Pe = 5$.

**Table 7.** The effect of $Nr$ for $Ra$ = $10^4$, $R_b$ = 10, $Pe$ = $Le$ = 1 in BC1 case.

| $Nr$ | $\psi_{min}$ | $\psi_{max}$ | $N_m^{max}$ | $\overline{Nu}$ | $\overline{Sh}$ | CPU (sec) |
|---|---|---|---|---|---|---|
| 0.1 | -3.60629 | 0.09052 | 1.00431 | 1.76114 | 0.27788 | 296.547 |
| 1 | -3.60155 | 0.16015 | 1.00498 | 1.72828 | 0.27992 | 295.766 |
| 5 | -3.69126 | 0.53483 | 1.00759 | 1.6276 | 0.28995 | 293.859 |
| 10 | -3.87712 | 0.97692 | 1.00980 | 1.56013 | 0.30226 | 296.672 |

**Table 8.** The effect of $R_b$ for $Ra = 10^4$, $Pe = Le = Nr = 1$ in BC1 case.

| $R_b$ | $\psi_{min}$ | $\psi_{max}$ | $N_m^{max}$ | $\overline{Nu}$ | $\overline{Sh}$ | CPU (sec) |
|---|---|---|---|---|---|---|
| 10 | -3.60155 | 0.16015 | 1.00498 | 1.72828 | 0.27992 | 295.766 |
| 25 | -2.99422 | 1.06071 | 1.01361 | 1.40527 | 0.31809 | 338.141 |
| 50 | -2.88191 | 1.69407 | 1.01763 | 1.31631 | 0.34454 | 304.906 |
| 100 | -2.97191 | 2.23903 | 1.01943 | 1.29994 | 0.36380 | 303.906 |

**Table 9.** The effect of $Pe$ for $Ra = 10^4$, $R_b = 10$, $Le = Nr = 1$ in BC1 case.

| $Pe$ | $\psi_{min}$ | $\psi_{max}$ | $N_m^{max}$ | $\overline{Nu}$ | $\overline{Sh}$ | CPU (sec) |
|---|---|---|---|---|---|---|
| 0.1 | -4.91876 | 0.00055 | 1.00008 | 2.23155 | 0.28478 | 311.375 |
| 1 | -3.60155 | 0.16015 | 1.00498 | 1.72828 | 0.27992 | 295.766 |
| 3 | -3.04006 | 1.08775 | 1.03944 | 1.40351 | 0.30096 | 298.547 |
| 5 | -3.00126 | 1.47416 | 0.70166 | 1.34561 | 0.30052 | 298.812 |

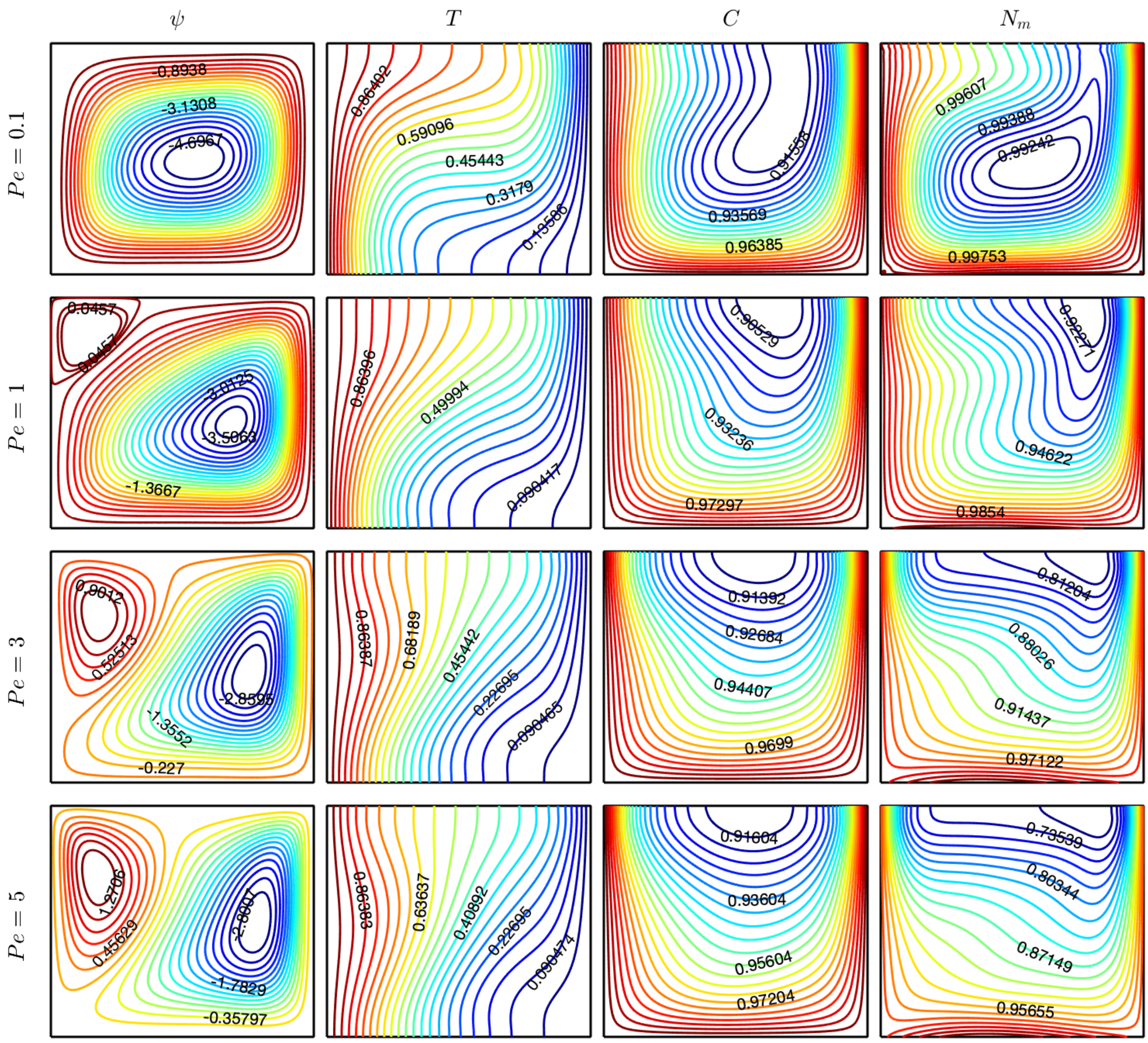

**Fig. 6.** The effect of $Pe$ for $Ra = 10^4$, $R_b = 10$, $Le = Nr = 1$ in BC1 case.

The heat transfer and fluid flow behavior are examined in distinct values of $Le$ number in Fig. 7. Lewis number is inversely proportional by diffusivity of nanoparticle concentration. As $Le$ number rises, the secondary cell disappears in streamlines, the thermal thin layers along the left and the right walls are getting thicker. Isoconcentration lying along the zero gradient top boundary moves to the center of the cavity, and forms more circulative behavior. Also, solutal boundary layers along the bottom and the right walls become thicker as $Le$ increases. Magnetotactic bacteria also move from the top wall to the center of the cavity as the diffusivity of nanoparticle concentration decreases. In Table 10, the accelerated fluid flow is noted with $\psi_{min}$ values as $Le$ increases. The maximum number of bacteria is decreasing from $Le = 1$ to $Le = 3$, but then it is not changing. Convective heat transfer is increasing 6.13 % from $Le = 1$ to $Le = 10$ due to the size of primary cell. A significant decrease occurs in convective mass transfer as 26.8 % reduction from $Le = 1$ to $Le = 10$ due to the reduction in concentration gradients along the left heated wall.

**Table 10.** The effect of *Le* for *Ra* = $10^4$, $R_b$ = 10, *Pe* = *Nr* = 1 in BC1 case.

| *Le* | $\psi_{min}$ | $\psi_{max}$ | $N_m^{max}$ | $\overline{Nu}$ | $\overline{Sh}$ | CPU (sec) |
|---|---|---|---|---|---|---|
| 1 | -3.60155 | 0.16015 | 1.00498 | 1.72828 | 0.27992 | 295.766 |
| 3 | -3.78891 | 0.01582 | 1.00000 | 1.74514 | 0.23198 | 303.875 |
| 6 | -4.09524 | 0.00418 | 1.00000 | 1.79885 | 0.21366 | 313.203 |
| 10 | -4.18966 | 0.00160 | 1.00000 | 1.83430 | 0.20498 | 313.547 |

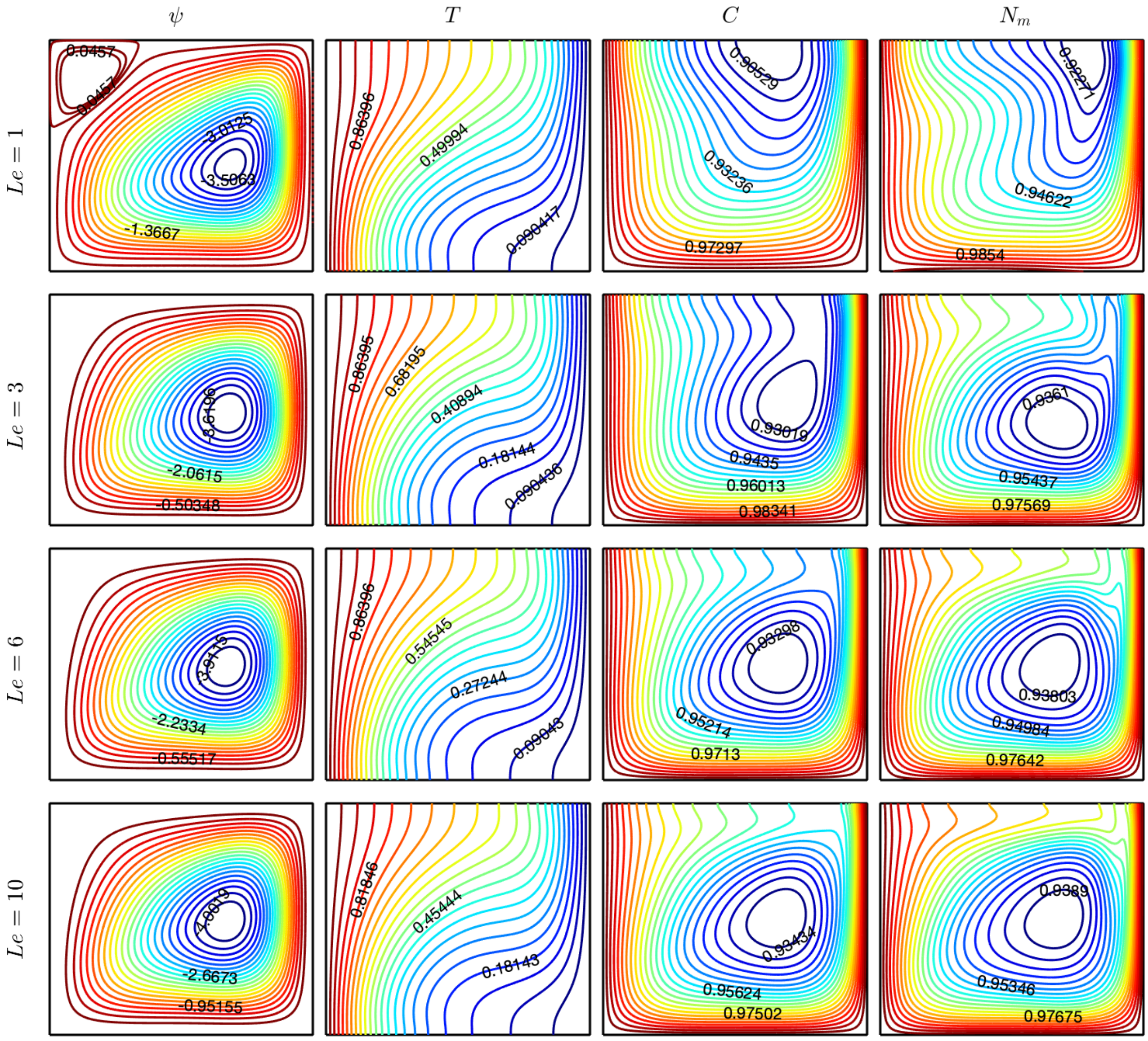


**Fig. 7.** The effect of *Le* for *Ra* = $10^4$, $R_b$ = 10, *Pe* = *Nr* = 1 in BC1 case.

### 4.4. BC 2

In this section, numerical results engaging the second boundary conditions are presented. In Fig. 8, Rayleigh number variation is detected keeping $R_b = 10$, $Pe = Le = Nr = 1$. In streamlines, symmetric cells at $Ra = 10^2$ are unified at $Ra = 10^3$, but then the secondary left cell gets larger at $Ra = 10^4$, and primary cell at $Ra = 10^4$ strongly circulate squeezing two cells through the left top and the right bottom corners. In isotherms, the thermal boundary layers along the vertical walls become prominent at $Ra = 10^5$ pointing to the buoyancy force dominance. Similar behavior is noted in isoconcentration lines due to the same boundary conditions as temperature. In magnetotactic bacteria isolines, smooth symmetric isolines at $Ra = 10^2$ as a result of the same boundary conditions of $N_m$ on vertical walls are distorted as $Ra$ rises. At $Ra = 10^4$, the right cell at $Ra = 10^3$ is sliding through the top and centralized close to the left wall while the left cell at $Ra = 10^3$ is suppressed by the right cell close to the bottom wall. At $Ra = 10^5$, movement of bacteria seems quicker than other $Ra$ values due to the strong circulation in isolines. In Table 11, as $Ra$ rises, the fluid velocity is escalated as well as $\overline{Nu}$ and $\overline{Sh}$. The number of bacteria also grows.

Figure 9 displays the influence of distinct buoyancy ratio number on fluid flow, the heat and mass transfer. In streamlines, primary cell at $Nr = 0.1$ is divided into secondary cell at $Nr = 1$, and the secondary cell dominates over primary cell at $Nr = 5$ and $Nr = 10$. In isotherms and in isoconcentration lines, the formation of thermal and solutal boundary layers along the left bottom and the right top part of vertical walls changes into the left top and the right bottom part at $Nr \geq 5$. In magnetotactic bacteria isolines, the symmetrically circulated cells at $Nr = 0.1$ are distorted at $Nr = 1$, and then symmetric formation is kept in the mid-left and in the mid-right part of the cavity at $Nr = 10$. In Table 12, $\overline{Nu}$ and $\overline{Sh}$ are increasing 83.4 % and 77.7 % from $Nr = 1$ to $Nr = 10$. Maximum number of bacteria grows 18.03 % as $Nr$ changed from 0.1 to 10.

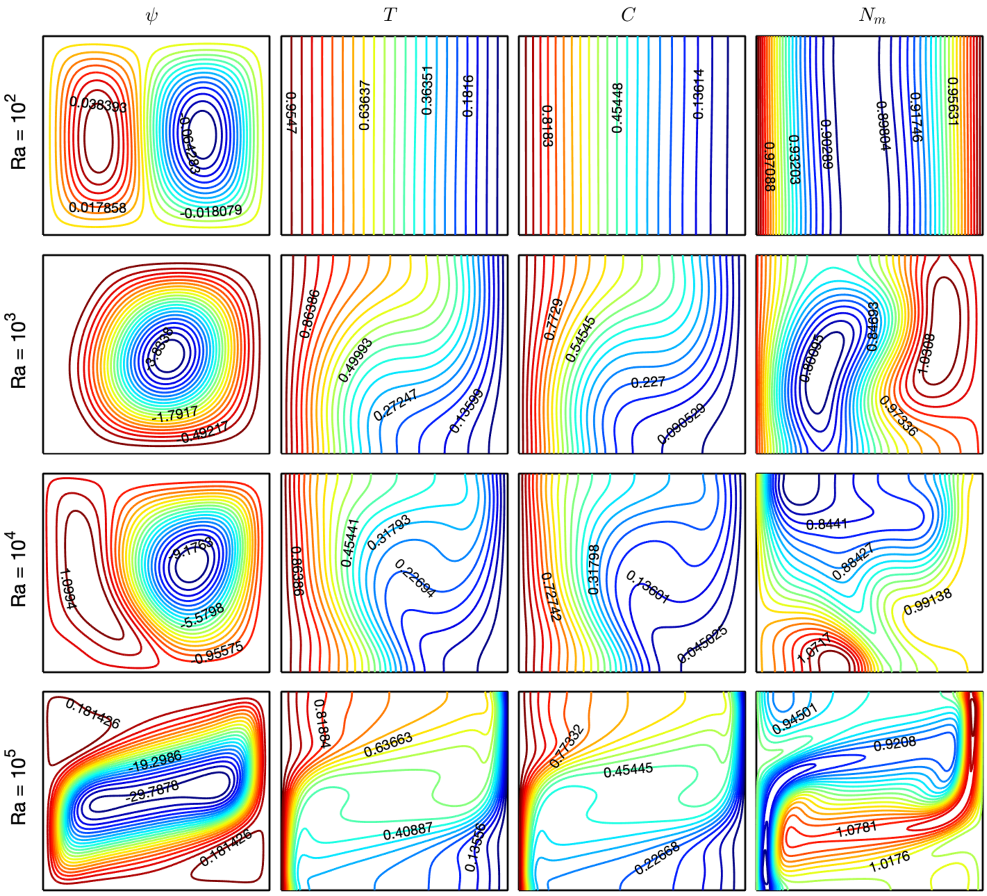


**Fig. 8.** The effect of *Ra* for $R_b$ = 10, *Pe* = *Le* = *Nr* = 1 in BC2 case.

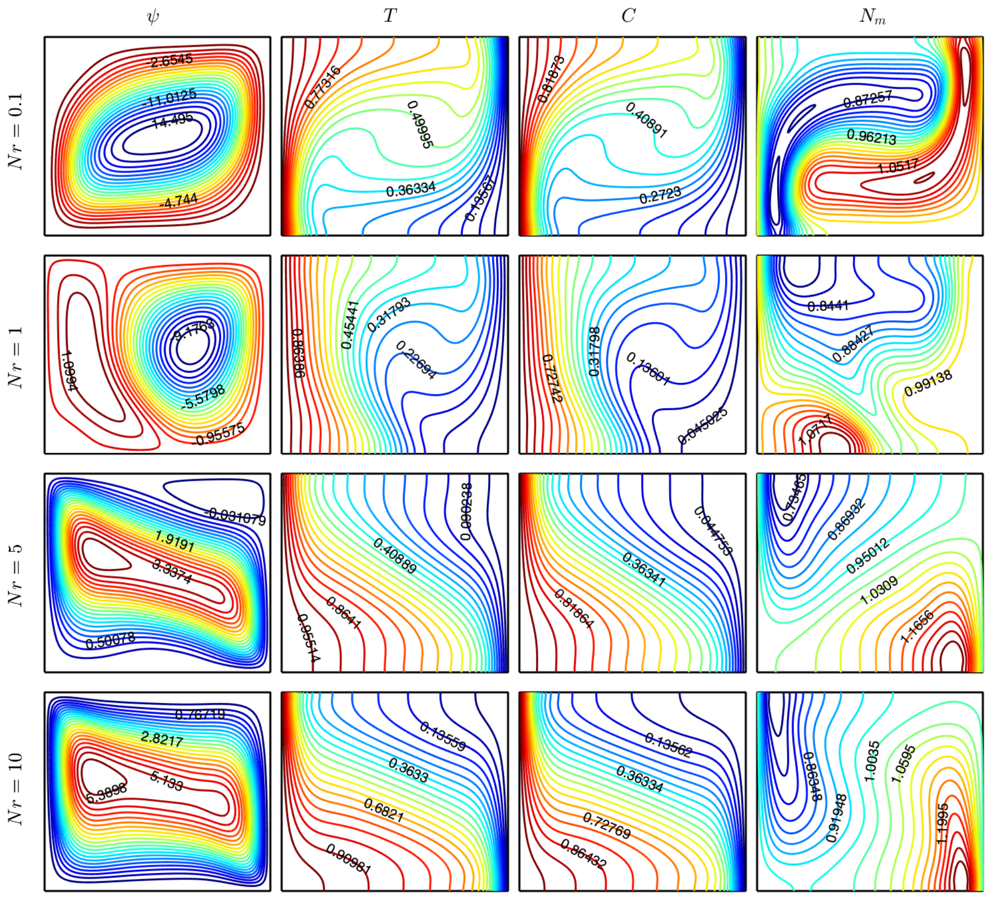


**Fig. 9.** The effect of *Nr* for *Ra* = $10^4$, $R_b$ = 10, *Pe* = *Le* = 1 in BC2 case.

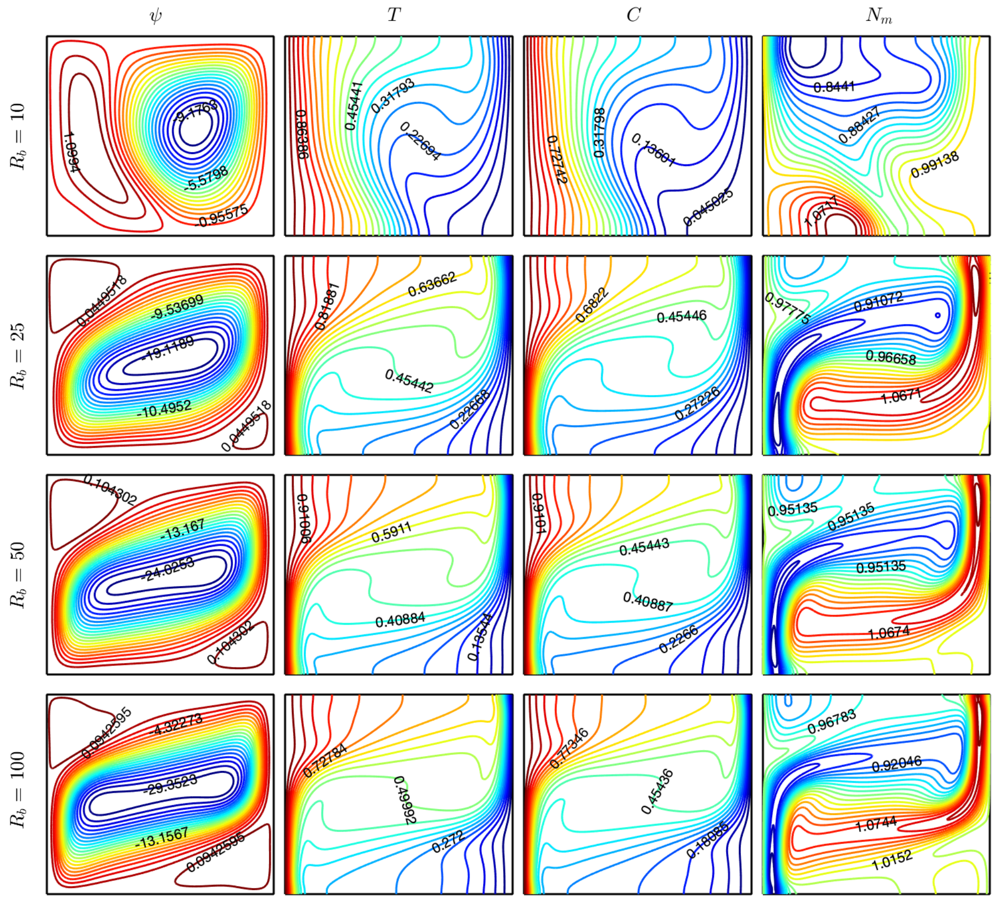


**Fig. 10.** The effect of $R_b$ for $Ra = 10^4$, $Pe = Le = Nr = 1$ in BC2 case.

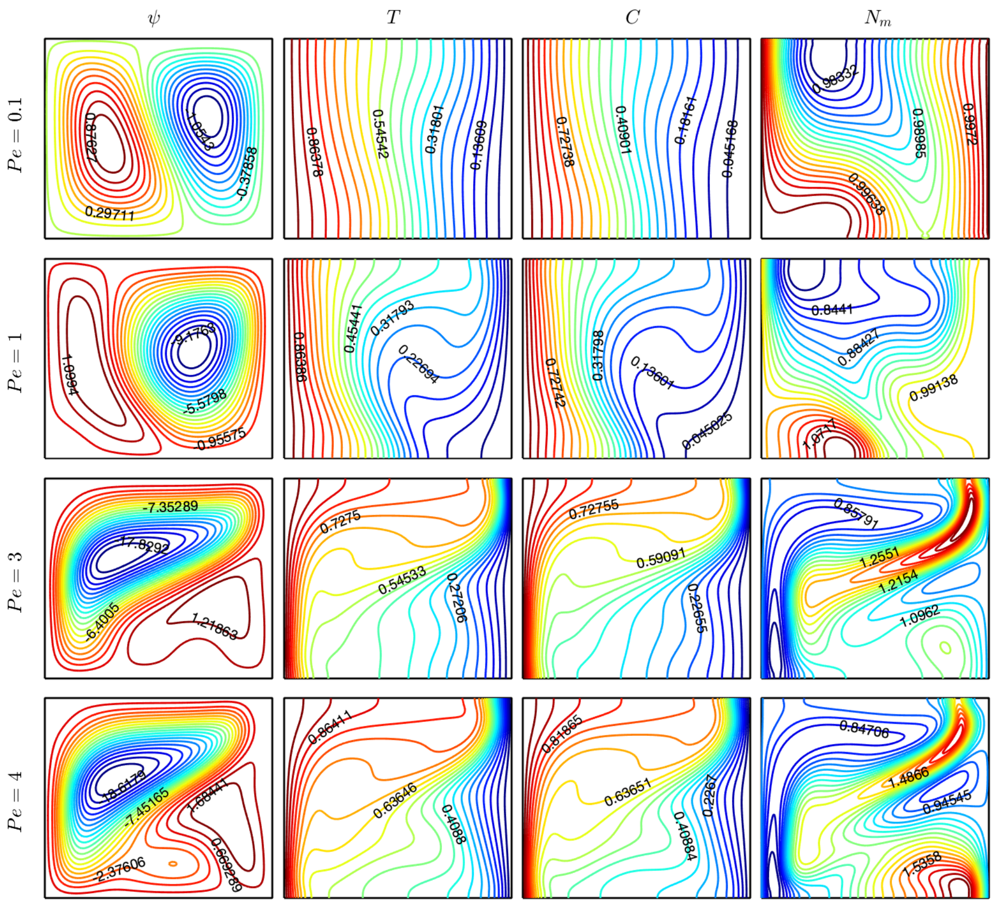


**Fig. 11.** The effect of $Pe$ for $Ra = 10^4$, $R_b = 10$, $Le = Nr = 1$ in BC2 case.

**Table 11.** The effect of $Ra$ for $R_b$ = 10, $Pe$ = $Le$ = $Nr$ = 1 in BC2 case.

| $Ra$ | $\psi_{min}$ | $\psi_{max}$ | $N_m^{max}$ | $\overline{Nu}$ | $\overline{Sh}$ | CPU (sec) |
|---|---|---|---|---|---|---|
| $10^2$ | -0.06939 | 0.04349 | 1.00000 | 1.04561 | 1.46317 | 329.891 |
| $10^3$ | -4.01466 | 0.06354 | 1.04223 | 1.59196 | 1.97898 | 1848.84 |
| $10^4$ | -9.67637 | 1.60667 | 1.09826 | 1.79492 | 2.11559 | 1083.44 |
| $10^5$ | -31.26678 | 1.66073 | 1.12645 | 5.96780 | 6.26365 | 3229.39 |

**Table 12.** The effect of $Nr$ for $Ra$ = $10^4$, $R_b$ = 10, $Pe$ = $Le$ = 1 in BC2 case.

| $Nr$ | $\psi_{min}$ | $\psi_{max}$ | $N_m^{max}$ | $\overline{Nu}$ | $\overline{Sh}$ | CPU (sec) |
|---|---|---|---|---|---|---|
| 0.1 | -15.18981 | 0.12959 | 1.09650 | 3.69266 | 4.06125 | 357.797 |
| 1 | -9.67637 | 1.60667 | 1.09826 | 1.79492 | 2.11559 | 1083.44 |
| 5 | -0.20724 | 3.69090 | 1.29962 | 2.13220 | 2.58365 | 308.266 |
| 10 | -0.00111 | 5.64616 | 1.33757 | 1.33757 | 3.75875 | 311.641 |

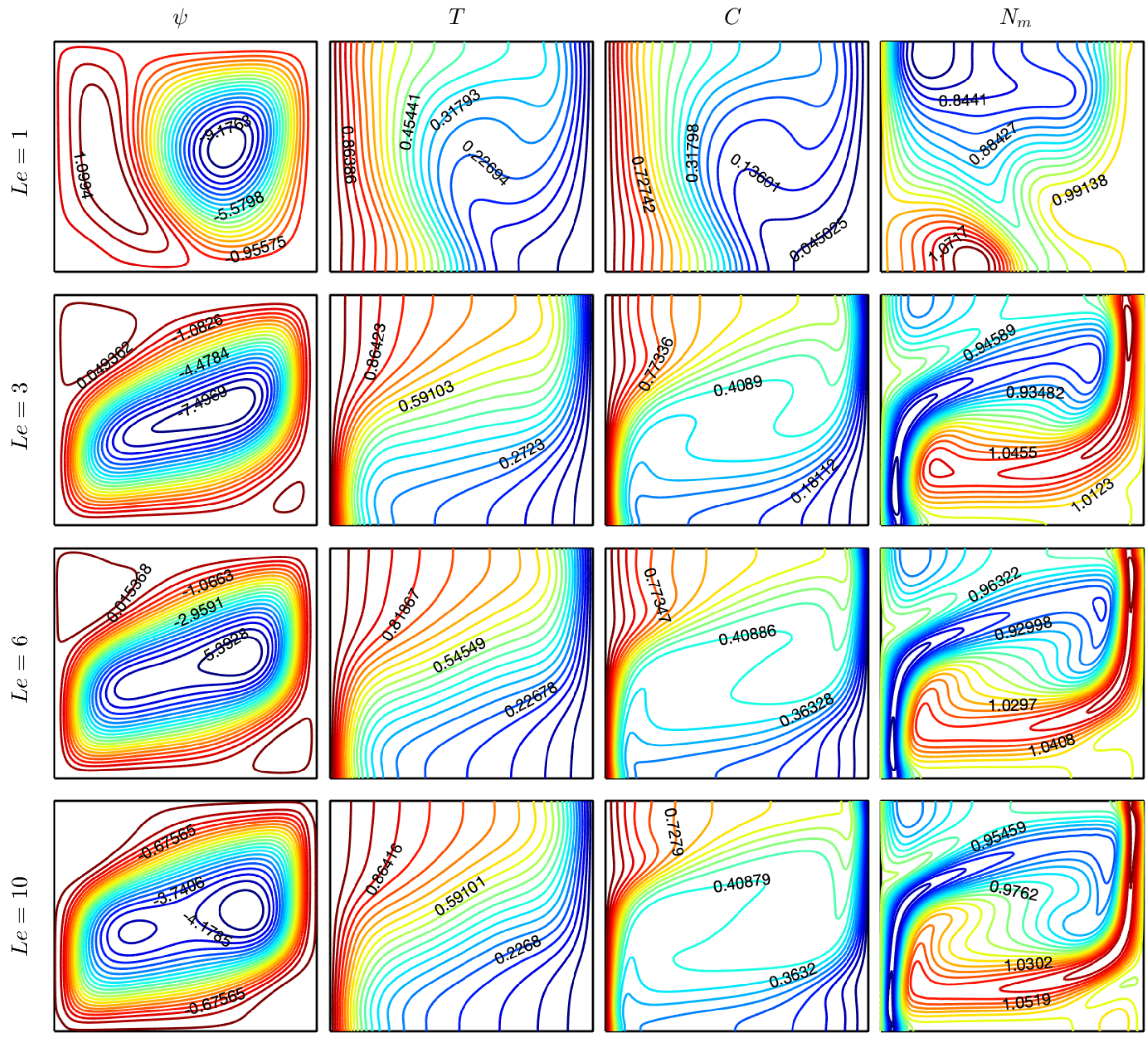


**Fig. 12.** The effect of $Le$ for $Ra$ = $10^4$, $R_b$ = 10, $Pe$ = $Nr$ = 1 in BC2 case.

In Fig. 10. the influence of bioconvection Rayleigh number is inquired when $Ra = 10^4$, $Pe = Le = Nr = 1$. With the rise in $R_b$, primary cell strongly circulates in streamlines, and the larger secondary cell at $R_b = 10$ is noted as smaller cells at larger $R_b$ numbers. The thermal and solutal boundary layers along the vertical walls display more convective behavior as $R_b$ rises. Similarly, bacteria move quicker inside at $R_b \geq 25$ than $R_b = 10$. In Table 13, rising $R_b$ is increasing $\overline{Nu}$ and $\overline{Sh}$ significantly. Maximum number of bacteria is almost not changing after $R_b \geq 50$.

The impact of different Peclet numbers is displayed in Fig. 11. In streamlines, the right primary cell at $Pe = 0.1$ is enlarged at $Pe = 1$, and the secondary cell disappears along the left wall while the new secondary cell emerges at the right bottom corner at $Pe = 3$ due to the effect of swimming bacteria. In isotherms, thermal and solutal boundary layer become noteworthy when $Pe$ is incremented from $Pe = 0.1$ to $Pe = 3$. From $Pe = 3$ to $Pe = 4$, the thick bold layers in isotherms and isoconcentration lines is decreasing a little bit. Strong up and down movement of bacteria inside the cavity occurs at $Pe = 3$ and $Pe = 4$ comparing to smaller $Pe$ numbers. In Table 14, the primary cell velocity is inflated by $Pe$ rise. Maximum number of bacteria increases 78.02 % from $Pe = 0.1$ to $Pe = 4$. $\overline{Nu}$ and $\overline{Sh}$ are elevated 217.8 % and 156.3 %, respectively, from $Pe = 0.1$ to $Pe = 3$.

**Table 13.** The effect of $R_b$ for $Ra = 10^4$, $Pe = Le = Nr = 1$ in BC2 case.

| $R_b$ | $\psi_{min}$ | $\psi_{max}$ | $N_m^{max}$ | $\overline{Nu}$ | $\overline{Sh}$ | CPU (sec) |
|---|---|---|---|---|---|---|
| 10 | -9.67637 | 1.60667 | 1.09826 | 1.79492 | 2.11559 | 1083.44 |
| 25 | -20.07496 | 1.00093 | 1.09576 | 4.59404 | 4.25086 | 929.141 |
| 50 | -25.20150 | 1.29395 | 1.11383 | 4.98627 | 5.30335 | 738.734 |
| 100 | -30.81649 | 1.54918 | 1.11974 | 5.68819 | 5.97834 | 1539.14 |

**Table 14.** The effect of $Pe$ for $Ra = 10^4$, $R_b = 10$, $Le = Nr = 1$ in BC2 case.

| $Pe$ | $\psi_{min}$ | $\psi_{max}$ | $N_m^{max}$ | $\overline{Nu}$ | $\overline{Sh}$ | CPU (sec) |
|---|---|---|---|---|---|---|
| 0.1 | -1.14893 | 0.97227 | 1.00046 | 1.09621 | 1.54671 | 412.328 |
| 1 | -9.67637 | 1.60667 | 1.09826 | 1.79492 | 2.11559 | 1083.44 |
| 3 | -18.76755 | 2.16540 | 1.61115 | 3.48359 | 3.96430 | 1156.22 |
| 4 | -19.60962 | 2.69175 | 1.78112 | 3.04442 | 3.61353 | 1889.5 |

**Table 15.** The effect of $Le$ for $Ra = 10^4$, $R_b = 10$, $Pe = Nr = 1$ in BC2 case.

| $Le$ | $\psi_{min}$ | $\psi_{max}$ | $N_m^{max}$ | $\overline{Nu}$ | $\overline{Sh}$ | CPU (sec) |
|---|---|---|---|---|---|---|
| 1 | -9.67637 | 1.60667 | 1.09826 | 1.79492 | 2.11559 | 1083.44 |
| 3 | -7.86962 | 0.42636 | 1.09975 | 3.04712 | 4.84755 | 1179.73 |
| 6 | -5.65879 | 0.28156 | 1.10639 | 2.72789 | 5.69232 | 1164.03 |
| 10 | -4.61143 | 0.20013 | 1.10160 | 2.48787 | 6.45911 | 603.922 |

**Table 16.** The effect of $\phi$ in different $Ra$ numbers keeping $R_b = 10$, $Pe = Le = Nr = 1$.

| | | BC1 | | | BC2 | | |
|---|---|---|---|---|---|---|---|
| $Ra$ | $\phi$ | $N_m^{max}$ | $\overline{Nu}$ | $\overline{Sh}$ | $N_m^{max}$ | $\overline{Nu}$ | $\overline{Sh}$ |
| $10^2$ | 0.01 | 1.00091 | 1.01268 | 0.34299 | 1.00000 | 1.02276 | 1.46318 |
| | 0.02 | 1.00089 | 1.02393 | 0.34302 | 1.00000 | 1.04561 | 1.46317 |
| | 0.03 | 1.00086 | 1.04669 | 0.34308 | 1.00000 | 1.06882 | 1.46316 |
| | 0.04 | 1.00084 | 1.06981 | 0.34314 | 1.00000 | 1.09239 | 1.46315 |
| $10^3$ | 0.01 | 1.00540 | 1.09756 | 0.32954 | 1.04282 | 1.58810 | 1.99666 |
| | 0.02 | 1.00537 | 1.11561 | 0.32999 | 1.04223 | 1.59196 | 1.97898 |
| | 0.03 | 1.00533 | 1.13419 | 0.33041 | 1.04161 | 1.59471 | 1.96053 |
| | 0.04 | 1.00529 | 1.15337 | 0.33088 | 1.04092 | 1.59623 | 1.94114 |
| $10^4$ | 0.01 | 1.00499 | 1.72535 | 0.27910 | 1.09870 | 1.78073 | 2.12901 |
| | 0.02 | 1.00498 | 1.72828 | 0.27992 | 1.09826 | 1.79492 | 2.11559 |
| | 0.03 | 1.00500 | 1.73100 | 0.28079 | 1.09775 | 1.80935 | 2.10261 |
| | 0.04 | 1.00503 | 1.73397 | 0.28168 | 1.09711 | 1.82398 | 2.09003 |

The effect of $Le$ number is inspected in Fig. 12. In streamlines, primary cell presses the secondary cell emerging at $Le = 1$ and is getting larger at $Le \geq 3$. The central vertex in streamlines at $Le = 3$ is divided into new cells pointing to a little bit decrease after $Le = 3$. Convective behavior in isotherms rises from $Le = 1$ to $Le = 3$ which are noted in strong thermal boundary layers along the vertical walls at $Le = 3$. This behavior is a little bit decreased after $Le = 3$. The $Le$ number is effective in concentration equation, and convective mass transfer in isoconcentration lines becomes stronger as $Le$ number increases. Magnetotactic bacteria circulate inside the cavity when $Le$ is ascended from $Le = 1$ to $Le = 3$, and then the circulation is almost the same. In Table 15, the decrease in fluid velocity in primary cell is confirmed by decreasing $\psi_{min}$ values. Maximum number of bacteria grows slowly from $Le = 1$ to $Le = 6$. Convective heat transfer increases 69.76 % from $Le = 1$ to $Le = 3$, and then decreases 18.35 % from $Le = 3$ to $Le = 10$. Convective mass transfer rises 205.3 % from $Le = 1$ to $Le = 10$. That is, mass transfer is significantly affected by the increase in $Le$ number.

In Table 16 the influence of the nanoparticle concentration affecting nanofluid properties is tested. Both in case of BC1 and BC2, convective heat transfer increases with the change in $\phi$ from 0.01 to 0.04. Convective mass transfer increases in BC1, however it is decreasing in BC2 if $\phi$ is incremented. This decrease in BC1 is gradually rise at larger $Ra$ numbers as $10^3$, $10^4$. In BC1, maximum number of bacteria is reduced with the augmentation in $\phi$ at $Ra = 10^3$, $10^4$ while a little bit increase is noted at $Ra = 10^4$. In BC2, $N_m^{max}$ is not changing at $Ra = 10^2$, but then it is a little bit decreasing at $Ra = 10^3, 10^4$.

## 5. Conclusion

In this study, natural convection flow in the presence of magnetotactic bacteria and $Fe_3O_4$ concentration inside $Fe_3O_4$-water nanofluid was numerically investigated. The dimensionless equations were solved by global RBF method using equally spaced points distributed inside the problem geometry. The problem was inquired in two distinct cases of boundary conditions examining the variation of Rayleigh, bioconvection Rayleigh, Peclet, Lewis numbers and buoyancy ratio parameter. Some remarkable points are:

In BC1 case,

- $N_m^{max}$ increases if $Nr$, $R_b$, $Pe$ $(0.1 \leq Pe \leq 3)$ increase, and it decreases as $Le$ rises from 1 to 3, but then it is not changing as $Le$ rises.
- $\overline{Nu}$ is decreasing as $Nr$, $R_b$, $Pe$ numbers increase (11.4 %, 24.9 %, 39.7%), and it is increasing as $Le$ and $Ra$ rise.
- $\overline{Sh}$ is increasing as $Nr$, $R_b$, $Pe$ $(1 \leq Pe \leq 5)$ increase, and it is decreasing as $Le$, $Ra$, $Pe$ $(0.1 \leq Pe \leq 1)$ increase.

In BC2 case,

- $N_m^{max}$ increases at any rise of $Ra$, $Nr$, $R_b$, $Pe$, $Le$ $(1 \le Le \le 6)$ parameters.
- $\overline{Nu}$ is increasing as $Ra$, $Nr$, $R_b$, $Pe$ $(0.1 \le Pe \le 3)$, $Le$ $(1 \le Le \le 3)$ rise.
- $\overline{Sh}$ is increasing as any parameter rise.

All in all, BC2 significantly affects the convective heat and mass transfer at any parameter growth. Maximum number of bacteria also exhibits increasing trend in BC2 comparing to BC1. In future, the presence of different nanoparticles with different bacteria types may be examined in more complex geometries including complex terms considering porous media or magnetic field effects. The challenges would be the adaptation of the used method to more complex geometries as well as different problem related parameter combinations.

## Author Contributions

Both authors contributed to the paper equally. The manuscript was written through the contribution of all authors. All authors discussed the results, reviewed, and approved the final version of the manuscript.

## Acknowledgments

Not applicable.

## Conflict of Interest

The authors declared no potential conflicts of interest concerning the research, authorship, and publication of this article.

## Funding

The authors received no financial support for the research, authorship, and publication of this article.

## Data Availability Statements

Data will be made available on request.

## Nomenclature

| | | | |
|---|---|---|---|
| $C$ | Concentration | $k$ | Thermal conductivity |
| $C_c$ | Concentration of cold wall | $n$ | Number of bacteria |
| $C_h$ | Concentration of hot wall | $n_0$ | Reference average number of bacteria |
| $C_{min}$ | Minimum concentration | $p$ | Pressure |
| $D_c$ | Diffusivity of nanoparticle concentration | $u$ | x-component of the velocity of the fluid |
| $D_n$ | Diffusivity of microorganism | $u_l$ | Characteristic velocity |
| $L$ | Characteristic length | $v$ | y-component of the velocity of the fluid |
| $Le$ | Lewis number, $\alpha_f / D_c$ | **Greek Letter** | |
| $Nr$ | Buoyancy ratio number, $(\rho_s - \rho_f)\beta_s \Delta C / (\rho_f \beta_f \Delta T)$ | $\alpha$ | Thermal diffusivity |
| $N_m$ | Nondimensional form of $n$ | $\beta$ | Thermal expansion coefficient |
| $Pe$ | Peclet number, $bW_c / D_n$ | $\gamma$ | Mean volume of microorganism |
| $Pr$ | Prandtl number, $\nu_f / \alpha_f$ | $\mu$ | Dynamic viscosity |
| $R_b$ | Bioconvection Rayleigh number $(\gamma \Delta\rho n_0) / (\rho_f \beta_f \Delta T)$ | $\nu$ | Kinematic viscosity |
| $Ra$ | Rayleigh number $g\beta_f \Delta T L^3 / (\nu_f \alpha_f)$ | $\rho$ | Fluid density |
| $T$ | Temperature | $\phi$ | Solid volume fraction |
| $T_c$ | Temperature of cold wall | $\psi$ | Stream function |
| $T_h$ | Temperature of hot wall | $\omega$ | Vorticity |
| $W_c$ | Maximum cell swimming speed | $\Delta\rho$ | Density difference |
| $\Delta C$ | Concentration difference | $\delta n'$ | $Fe_3O_4$ consumption |
| $\Delta T$ | Temperature difference | **Subscript** | |
| $\overline{Nu}$ | Average Nusselt number | $f$ | Fluid |
| $\overline{Sh}$ | Average Sherwood number | $nf$ | Nanofluid |
| $b$ | Chemotaxis constant | $s$ | Solid |
| $g$ | Gravitational acceleration | | |

## References

[1] Hayat, T., Rai, S., Ahmed, A., Taseer M., Rahmat, E., On squeezed flow of couple stress nanofluid between two parallel plates, *Results in Physics*, 7, 2017, 553-561.
[2] Choi, S.U.S., Eastman, A.J., Enhancing thermal conductivity of fluids with nanoparticles, *Argonne National Laboratory (ANL)*, Argonne, IL, United States, 1995.
[3] Khanafer, K., Vafai, K., Lightstone, M., Buoyancy-driven heat transfer enhancement in a two-dimensional enclosure utilizing nanofluids, *International Journal of Heat and Mass Transfer*, 46(19), 2003, 3639-3653.
[4] Jou, R.Y., Tzeng, S.C., Numerical research of nature convective heat transfer enhancement filled with nanofluids in rectangular enclosures, *International Communications in Heat and Mass Transfer*, 33, 2006, 727-736.
[5] Kefayati, G.H.R., Lattice Boltzmann simulation of natural convection in nanofluid-filled 2D long enclosures at presence of magnetic field, *Theoretical and Computational Fluid Dynamics*, 27(6), 2013, 865-883.
[6] Pekmen Geridonmez, B., RBF simulation of natural convection in a nanofluid-filled cavity, *AIMS Mathematics*, 1(3), 2016, 195-207.
[7] Bhuiyana, A.H., Shahidul, Md.A., Alim, M.A., Natural convection of water-based nanofluids in a square cavity with partially heated of the bottom wall, *Procedia Engineering,* 194, 2017, 435-441.
[8] Joshi, P.S., Pattamatta, A., Enhancement of natural convection heat transfer in a square cavity using MWCNT/Water nanofluid: an experimental study, *Heat and Mass Transfer*, 54, 2018, 2295-2303.
[9] Mousavi, S.B., Heris, S.Z., Hosseini, M.G., Experimental investigation of MoS2/diesel oil nanofluid thermophysical and rheological properties, *International Communications in Heat and Mass Transfer*, 108, 2019, 104298.
[10] Alsabery, I.A., Gedik, E., Chamkha, A.J., Hashim, I., Impacts of heated rotating inner cylinder and two-phase nanofluid model on entropy generation and mixed convection in a square cavity, *Heat and Mass Transfer*, 56(1), 2020, 321-338.
[11] Mousavi, S.B., Heris, S.Z., Estellé, P., Experimental comparison between ZnO and MoS2 nanoparticles as additives on performance of diesel oil-based nano lubricant, *Scientific Reports*, 10(1), 2020, 5813.
[12] Mousavi, S.B., Heris, S.Z., Experimental investigation of ZnO nanoparticles effects on thermophysical and tribological properties of diesel oil, *International Journal of Hydrogen Energy*, 45(43), 2020, 23603-23614.
[13] Mousavi, S.B., Heris, S.Z., Estellé, P., Viscosity, tribological and physicochemical features of ZnO and MoS2 diesel oil-based nanofluids: An experimental study, *Fuel*, 293, 2021, 120481.
[14] Sarvari, A.A., Heris, S.Z., Mohammadpourfard, M., Mousavi, S.B., Estellé, P., Numerical investigation of TiO2 and MWCNTs turbine meter oil nanofluids: Flow and hydrodynamic properties, *Fuel*, 320, 2022, 123943.
[15] Pourpasha, H., Heris, S.Z., Mousavi, S.B., Thermal performance of novel ZnFe2O4 and TiO2-doped MWCNT nanocomposites in transformer oil, *Journal of Molecular Liquids*, 394, 2024, 123727.
[16] Khouri, O., Goshayeshi, H.R., Mousavi, S.B., Hosseini Nami, S., Zeinali Heris, S., Heat Transfer Enhancement in Industrial Heat Exchangers Using Graphene Oxide Nanofluids, *ACS Omega*, 9, 2024, 24025-24038.
[17] Mousavi, S.B., Pourpasha, H., Heris, S.Z., High-temperature lubricity and physicochemical behaviors of synthesized Cu/TiO2/MnO2-doped GO nanocomposite in high-viscosity index synthetic biodegradable PAO oil, *International Communications in Heat and Mass Transfer*, 156, 2024, 107642.
[18] Luong, D., Sau, S., Kesharwani, P., Iyer, A.K., Polyvalent folate-dendrimer-coated iron oxide theranostic nanoparticles for simultaneous magnetic resonance imaging and precise cancer cell targeting, *Biomacromolecules*, 18, 2017, 1197-1209.
[19] Dave, P.N., Chopda, L.V., Application of iron oxide nanomaterials for the removal of heavy metals, *Journal of Nanotechnology*, 2014(1), 398569.
[20] Sundar, S.L., Singh, K.M., Sousa, C.M.A., Investigation of thermal conductivity and viscosity of Fe3O4 nanofluid for heat transfer applications, *International Communications in Heat and Mass Transfer,* 44, 2013, 7-14.
[21] Moraveji, M.K., Majid, H., Natural convection in a rectangular enclosure containing an oval-shaped heat source and filled with Fe3O4/water nanofluid, *International Communications in Heat and Mass Transfer*, 44, 2013, 135-146.
[22] Acharya, N., On the flow patterns and thermal control of radiative natural convective hybrid nanofluid flow inside a square enclosure having various shaped multiple heated obstacles, *The European Physical Journal Plus*, 136(8), 2021, 889.
[23] Acharya, N., Finite element analysis on the hydrothermal pattern of radiative natural convective nanofluid flow inside a square enclosure having nonuniform heated walls, *Heat Transfer,* 51(1), 2022, 323-354.
[24] Acharya, N., Impacts of different thermal modes of multiple obstacles on the hydrothermal analysis of Fe3O4–water nanofluid enclosed inside a nonuniformly heated cavity, *Heat Transfer*, 51(2), 2022, 1376-1405.
[25] Tekir, M., Taskesen, E., Gedik, E., Arslan K., Aksu, B., Effect of constant magnetic field on Fe3O4-Cu/water hybrid nanofluid flow in a circular pipe, *Heat and Mass Transfer,* 58, 2022, 707–717.
[26] Eshgarf, H., Nadooshan, A.A., Raisi, A., Afrand, M., Experimental examination of the properties of Fe3O4/water nanofluid, and an estimation of a correlation using an artificial neural network, *Journal of Molecular Liquids*, 374, 2023, 121150.
[27] Acharya, N., Hydrothermal scenario of buoyancy-driven magnetized multi-walled carbon nanotube-Fe3O4-water hybrid nanofluid flow within a discretely heated circular chamber fitted with fins, *Journal of Magnetism and Magnetic Materials*, 589, 2024, 171612.
[28] Acharya, N., Magnetically driven MWCNT-Fe3O4-water hybrid nanofluidic transport through a micro-wavy channel: a novel MEMS design for drug delivery application, *Materials Today Communications*, 38, 2024, 107844.
[29] Alloui, Z., Nguyen T.H., Bilgen E., Numerical investigation of thermobioconvection in a suspension of gravitactic microorganisms, *International Journal of Heat and Mass Transfer*, 50(7-8), 2007, 1435-1441.
[30] Kuznetsov, A.V., The onset of nanofluid bioconvection in a suspension containing both nanoparticles and gyrotactic microorganisms, *International Communications in Heat and Mass Transfer*, 37(10), 2010, 1421-1425.
[31] Kuznetsov, A.V., Nanofluid bioconvection: interaction of microorganisms oxytactic upswimming, nanoparticle distribution, and heating/cooling from below, *Theoretical and Computational Fluid Dynamics*, 26, 2012, 291-310.
[32] Sheremet M.A., Pop, I., Thermo-bioconvection in a square porous cavity filled by oxytactic microorganisms, *Transport in Porous Media*, 103, 2014, 191-205.
[33] Md Basir, M.F., Uddin, M.J., Md Ismail, A.I., Bég, O.A., Nanofluid slip flow over a stretching cylinder with Schmidt and Péclet number effects, *AIP Advances*, 6(5), 2016, 055316.
[34] Saini, S., Sharma, Y.D., Numerical study of nanofluid thermobioconvection containing gravitactic microorganisms in porous media: Effect of vertical through flow, *Advanced Powder Technology,* 29(11), 2018, 2725-2732.
[35] Habibishandiz, M., Saghir, Z., Zahmatkesh, I., Thermo-bioconvection performance of nanofluid containing oxytactic microorganisms inside a square porous cavity under constant and periodic temperature boundary conditions, *International Journal of Thermofluids*, 17, 2023, 100269.
[36] Bazylinski, A.D., Frankel, B.R., Heywood, B.R., Mann, S., King, J.W., Donaghay, L.P., Hanson, A.K., Controlled Biomineralization of Magnetite (Fe3O4) and Greigite (Fe3S4) in a Magnetotactic Bacterium, *Applied and Environmental Microbiology*, 61(9), 1995, 3232-3239.
[37] Fouladi, J., Lu, Z., Yvon S., Sylvain, M., An integrated biosensor for the detection of bio-entities using magnetotactic bacteria and CMOS technology, *In 2007 29th Annual International Conference of the IEEE Engineering in Medicine and Biology Society,* 2007.
[38] Benoit, M.R., Mayer, D., Yoram, B., Chen, I.Y., Hu, W., Cheng, Z., Wang, X.S., Spielman, D.M., Gambhir, S.S., Matin, A., Visualizing implanted tumors in mice with magnetic resonance imaging using magnetotactic bacteria, *Clinical Cancer Research*, 15(16), 2009, 5170-5177.
[39] Song, H.P., Li, X.G., Sun, J.S., Xu S.M., Xu, H., Application of a magnetotactic bacterium, Stenotrophomonas sp. to the removal of Au (III) from contaminated wastewater with a magnetic separator, *Chemosphere*, 72(4), 2008, 616-621.
[40] Ali, I., Changsheng, P., Khan, Z.M., Naz, I., Sultan, M., An overview of heavy metal removal from wastewater using magnetotactic bacteria, *Journal of Chemical Technology & Biotechnology*, 93(10), 2018, 2817-2832.
[41] Pekmen Geridonmez, B., Oztop, H.F., Magnetotactic bacteria and Fe3O4-water in a wavy walled cavity, *International Journal of Numerical Methods for Heat & Fluid Flow*, 34, 2024, 1609-1630.
[42] Maxwell, J.C.C., Colours in metal glasses and in metallic films, *Philosophical Transactions of the Royal Society of London, Series A*, 203, 1904, 385-420.
[43] Brinkman, C.H., The viscosity of concentrated suspensions and solutions, *The Journal of Chemical Physics*, 20, 1952, 571–571.
[44] Kuznetsov, A.V., Thermo-bioconvection in a suspension of oxytactic bacteria, *International Communications in Heat and Mass Transfer*, 32(8), 2005, 991–

999.
[45] Reddy, N., Murugesan, K., Magnetic field influence on double-diffusive natural convection in a square cavity - A numerical study, *Numerical Heat Transfer, Part A: Applications*, 71(4), 2017, 448-475.
[46] Balla, C.S., Haritha, C., Kishan K., Rashad, A.M., Bioconvection in nanofluid-saturated porous square cavity containing oxytactic microorganisms, *International Journal of Numerical Methods for Heat & Fluid Flow*, 29(4), 2019, 1448-1465.
[47] Teamah, M.A., Numerical simulation of double diffusive natural convection in rectangular enclosure in the presences of magnetic field and heat source, *International Journal of Thermal Sciences,* 47(3), 2008, 237-248.
[48] Ghachem, K., Kolsi, L., Maatki, C., Hussein, A.K., Mohamed Naceur, B., Numerical simulation of three-dimensional double diffusive free convection flow and irreversibility studies in a solar distiller, *International Communications in Heat and Mass Transfer,* 39(6), 2012, 869-876.
[49] Fasshauer, E.G., *Meshfree approximation methods with MATLAB*, World Scientific, 2007.
[50] Fasshauer, E.G., McCourt, M.J., *Kernel-based approximation methods using Matlab*, World Scientific Publishing Company, 2015.
[51] Vahl Davis, G., Natural convection of air in a square cavity: a bench mark numerical solution, *International Journal for Numerical Methods in Fluids*, 3(3), 1983, 249-264.
[52] Ho, C.J., Liu, W.K., Chang, Y.S., Lin, C.C., Natural convection heat transfer of alumina-water nanofluid in vertical square enclosures: An experimental study, *International Journal of Thermal Sciences*, 49(8), 2010, 1345-1353.
[53] Saghir, M.Z., Ahadi, A., Mohamad, A., Srinivasan, S., Water aluminum oxide nanofluid benchmark model, *International Journal of Thermal Sciences*, 109, 2016, 148-158.

## ORCID iD

Merve Gurbuz-Caldag https://orcid.org/0000-0002-7746-9005
Bengisen Pekmen https://orcid.org/0000-0002-3073-6284



**How to cite this article:** Gurbuz-Caldag M., Pekmen B. Numerical Investigation on Fe3O4-Water Nanofluid in the Presence of Magnetotactic Bacteria, *J. Appl. Comput. Mech.*, 11(2), 2025, 467-484. https://doi.org/10.22055/jacm.2024.47204.4674